Investigation of the Operation of Resistive Plate Chambers

THE UNIVERSITY
of MANCHESTER

Jane T. Bromley

Department of Physics and Astronomy

A thesis submitted to the University of Manchester for the degree of Master of Science in the Faculty of Science and Engineering.

September, 1994

Contents

List of Figures

Abstract

The properties of various resistive plate chambers were investigated with particular regard to their suitability for use as a fast muon trigger system in the expected environment of future high energy particle colliders. Two distinct classes of pulses were observed: a class of small pulses (the avalanche mode), and a class of large pulses (the streamer mode). Evidence was found for a transition between the two modes. The efficiencies of the chambers were measured. The variations in the shape and timing characteristics of the read-out pulses were examined with changes in chamber parameters.

Declaration

No portion of the work referred to in this thesis has been submitted in support of an application for another degree or qualification of this or any other university or other institute of learning.

1. Copyright in text of this thesis rests with the Author. Copies (by any process) either in full, or of extracts, may be made only in accordance with instructions given by the Author and lodged in the John Rylands University Library of Manchester. Details may be obtained from the Librarian. This page must form part of any such copies made. Further copies (by any process) of copies made in accordance with such instructions may not be made without the permission (in writing) of the Author.

2. The ownership of any intellectual property rights which may be described in this thesis is vested in the University of Manchester, subject to any prior agreement to the contrary, and may not be made available for use by third parties without the written permission of the University, which will prescribe the terms and conditions of any such agreement.

Further information on the conditions under which disclosures and exploitation may take place is available from the Head of Department of Physics and Astronomy.

Chapter 1

Introduction

1.1 History

The Resistive Plate Chamber (or Counter) (RPC) was first developed in 1981 by Santonico and Cardarelli [1], as a fast detector which might be able to cover large areas economically. It is a variant of the widespread parallel plate and spark chambers in which a homogeneous electric field is applied across two parallel resistive plates enclosing a gas gap. Particles passing through lead to ionisation and avalanching in the gas towards the electrodes and thence to a detectable signal. Various properties have been reported for RPCs which make them viable for use as muon detectors, and especially for use as a muon trigger, these are [2]:

- large-scale area coverage
- prompt detection of particles
- time resolution $\sigma_t \sim 1.8$ ns
- relatively simple construction and operation
- low cost

RPCs have been used with success in the past: as a fast tracking muon trigger in WA92 [3] and E771 [4], and as a muon detector in Soudan 2 [5]. The

results from these experiments showed some problems with a drop in RPC efficiency at higher flux rates, but in spite of this potential drawback RPCs are under consideration for use in a dedicated muon trigger for the ATLAS (A Toroidal LHC ApparatuS) experiment (see fig. **??**) planned for the future Large Hadron Collider (LHC) at CERN.

1.2 The LHC and ATLAS

The LHC is a proton proton collider designed to reach centre of mass energies of about 14 TeV in order to search for physics beyond the standard model, such as supersymmetric particles and the Higgs boson. One of the most important items at LHC is the detection of the 4μ decay channel of the Higgs boson. A low signal to background ratio is expected, so that a high luminosity is required in order to ensure the production of at least a few events a year. LHC hopes to operate at a peak luminosity of 1.7×10^{34} cm^{-2}s^{-1}, with a bunch-spacing of 25ns [6]. Detectors working in such an environment need to be able to cope with the exceptionally high and constant levels of ionisation. The most important requirement for a detector involved in the trigger logic is the ability to provide the necessary timing with the precision to separate interactions coming from two consecutive bunches.

1.2.1 The ATLAS muon trigger

In order to be able to satisfy the physics requirements of the detector, the ATLAS muon trigger must possess the capability to trigger on muons with transverse momenta between very low (p_T = 6 GeV/c, for B physics) and high (p_T = 40 GeV/c, for heavy boson searches) values. It will be necessary for the trigger to operate reliably up to high luminosity and to show a suitable redundancy with respect to background. There must be some adaptability in the design to cope with unexpected situations, such as the possibility of needing to veto various areas of the detector, and it is important that the trigger system should not affect the

performance of the precision tracking chambers adversely (as may happen with the addition of extra material for for dedicated trigger chambers) [7].

The ATLAS Muon Review Panel has decided on a dedicated muon system - i.e. to have separate detectors dedicated to the trigger alone, rather than a trigger derived from the tracking detectors. Two layers of trigger chambers are thought to be necessary to provide sufficient robustness against background.

The proposed trigger system uses a combination of two types of detectors: Resistive Plate Chambers and Thin Gap Chambers (TGCs). The RPC is seen as a good option for the barrel region, where its rate capability is an order of magnitude larger than the expected soft particle background. The TGC, with a slightly worse time resolution but better rate capability, is a good solution for the forward high rapidity region.

The strong points of the RPC are seen as being its ease of construction on an industrial scale, and the experience already gained in this area, and its fast rise-time. Its weak point is its rate capability, which has yet to be shown to be sufficient for LHC operation.

Important progress has recently been made in improving the rate capability of RPCs by decreasing the gas amplification and increasing the amplification of the front-end electronics [8]. An RPC operating with such a low gas amplification has been tested in RD5 [9, 10]. It exhibited an improvement of one order of magnitude in rate capability. The operating mode has the following features:

- signal charge < 1 pC;
- rate capability $\simeq 1$ kHz/cm^2;
- time resolution 1.3 ns at 100 Hz/cm^2 and 1.8 ns at 1 kHz/cm^2;
- negligible increase of the delay with the counting rate (1 ns/kHz);
- absence of non gaussian tails in the time jitter distributions.

At a luminosity, $\mathcal{L}$, of 1×10^{33} cm^{-2} s^{-1} the expected average counting rate is about 4 Hz/cm^2. Considerable progress has been made in demonstrating certain performance specifications, which need to be satisfied for use of these chambers as the muon trigger. It is planned to extend these studies by building and equipping full-size chambers and testing them in conjunction with the muon tracking chambers (Monitored Drift Tubes) in the test beam. Studies on particle rates have been encouraging, but will need to be extended to irradiation of full-size chambers. Plans also include the continuation of extensive radiation damage tests.

Chapter 2

Design and operation

2.1 Basic design

The basic design of an RPC is shown in fig 2.1. Essentially it consists of two parallel resistive plates about 2mm thick, separated by a gas gap whose width is maintained by spacers. The gas is kept at atmospheric pressure and a DC voltage is applied to the plates via a layer of graphite paint on their external surface. The graphite electrodes are covered with an insulating layer of PCB on which is etched a thin layer of copper which acts as a pickup pad to detect any movement of charge within the chamber.

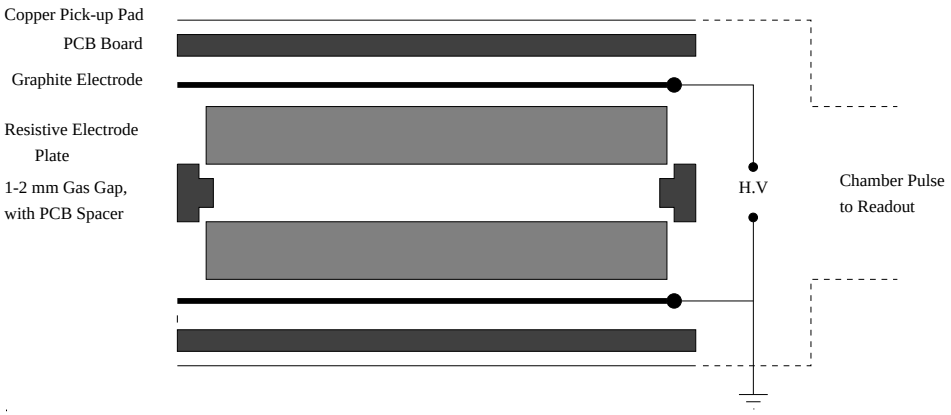

Figure 2.1: The basic RPC design.

The narrowness of the gas gap (as compared with a drift chamber for instance) means that a very intense and uniform electric field can be sustained. Chambers of this kind can be made easily and cheaply, and hence are a particularly viable alternative for muon detection given the need for large area coverage and adequate temporal and spatial resolution.

There are two distinct classes of pulse:

- Avalanche (or proportional) mode (see fig. 2.2) - in which only small (< 10 mV on 50 Ω) pulses are seen. These arrive promptly after the through-passage of the initial ionising particle, have a risetime of 10-15 ns, and a total pulse length of around 50 ns. The total charge observed is of the order of 1 pC.

- Streamer (or Spark) mode (see fig. 2.3) - where the pulses are large, ($\geq$ 100 mV on 50 Ω)[1], deposit a charge of about 100 pC, and have a greater spread of arrival times (from prompt arrival up to 200 ns after the initial ionising particle). The signals have risetimes of the order of 10 ns and pulse lengths between 100-500 ns (500 ns for a multipulsing event). These streamer pulses are generally preceded by a small prepulse - the contention is that this prepulse is an avalanche pulse which subsequently builds up enough charge to trigger the streamer. Double, triple, and multi-pulses are also seen (see fig. 2.3) - and these become increasingly common as a chamber nears breakdown.

Chapter 6 has further data on pulse-shapes and sizes for the two modes of operation. Other sources, for instance RD5 [9], have claimed much faster rise-times (of the order of 1.5 ns) for their streamer pulses: those reported here are an order of magnitude slower. However RD5 were using strip RPCs with a pitch of 0.78 cm and a low gas amplification, whilst the Manchester chambers consist of undivided plates of 6×6 cm^2 area using a relatively high gas amplification, so it seems likely that the origin of this discrepancy is a combination of the large read-out area of the Manchester chambers and the larger gas amplification of the pulses.

[1] One of the original selling points of the RPC was that these large pulses avoided the need for preamplification before logic.

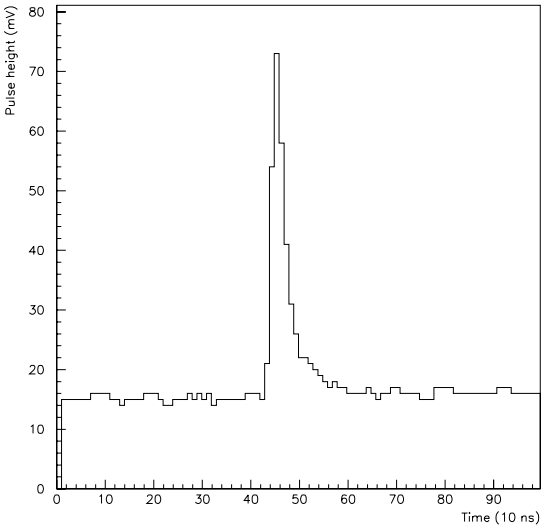

Figure 2.2: An FADC digitising of an amplified ($\times 10$) avalanche pulse.

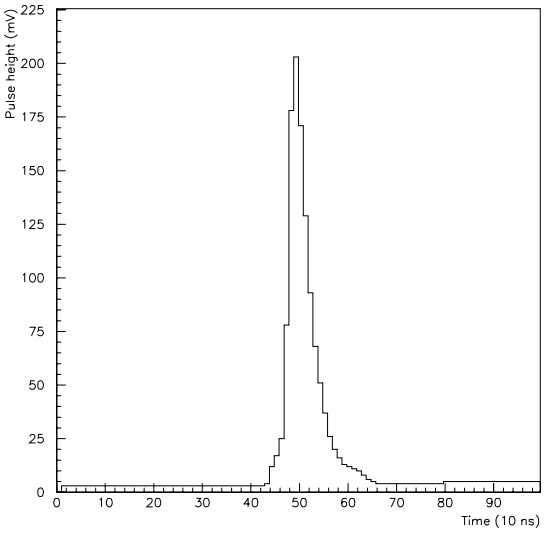

Figure 2.3: An FADC digitising of a streamer pulse.

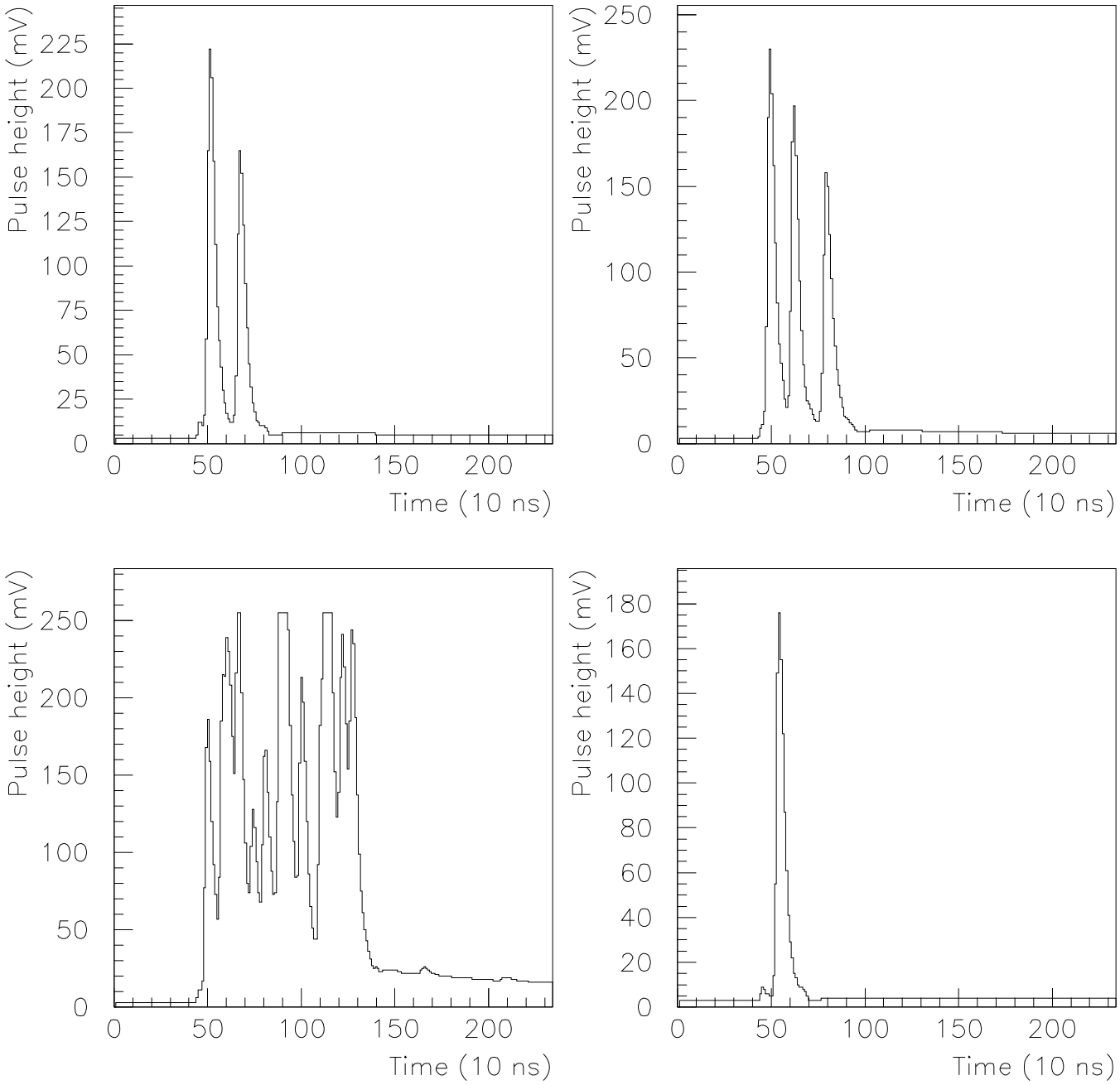

Figure 2.4: Examples from an RPC with a 4mm gas gap of a) a double pulse, b) a triple pulse, c) a multipulse, and d) a streamer preceded by a pre-pulse.

2.2 Principles of operation

The RPC operates, as do other gas detectors, using the gas multiplication of ions and electrons left in the gap by the passage of a charged particle through the chamber. For a gas mixture of 70% argon and 30% isobutane (similar to the gas mixtures used in the operation of many RPCs) a relativistic minimum ionising particle passing through the gas produces on average a primary ionisation of 34 ion pairs/cm - this process follows a Poisson distribution. Some of the free electrons formed in this way possess enough energy to produce further ionisation, hence increasing the total average ionisation to 124 ion pairs/cm [11]. In this way clusters of electrons and ions are produced around the primary ionisation events.

The high electric field in the gap causes the charged clusters to drift towards the electrodes. Due to their much lower mass, the electrons have a significantly higher drift velocity ($\sim 10^7$ cm s^{-1}) than the more lethargic positively charged ions (which move in the opposite direction at approximately 10^5 cm s^{-1}) and accelerate towards the anode, ionising yet more molecules in their path. The process continues and an electron avalanche develops towards the anode, its growth controlled by the Townsend equation:

$$n = e^{\alpha x}$$

where n is the number of electrons produced in the path of a single electron travelling a distance x; and α is the first Townsend coefficient,which can be derived crudely using kinetic theory [12] as

$$\alpha = Ape^{-\frac{Bp}{E}}$$

where A and B are constants, p is the gas pressure, and E the electric field.

Photographs of avalanches in wire chambers [13] show that they tend to be wedge-shaped with a rounded head - somewhat like elongated droplets (as in fig 2.5). The length is dictated by the electron drift velocity in the field, and the radius by the electron diffusion ($r^2 = 4Dt$).

Many avalanches remain at this stage of development and merely continue

to grow towards the anode until they reach it, at which point the charge in the avalanche is deposited on the resistive plate. The deposited charge flows away into the plate.

However, the avalanche process may continue until there are of the order of 10^8 electrons in the head of the avalanche, at which point it is thought that space charge effects become dominant and a streamer-type mechanism takes over. There has been some disagreement over the mechanism of streamer development, particularly with reference to the transition between avalanche and streamer modes of discharge; but the most likely model [14] can be summed up as follows.

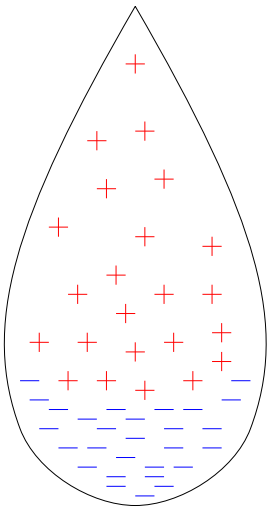

Figure 2.5: A schematic diagram of an avalanche.

As the avalanche progresses the space-charge fields of the clouds of electrons and positive ions becomes important. When the number of electrons in the advancing head of the avalanche approaches 10^6 the avalanche begins to slow down due to the attraction of the positive ions; when the number reaches 10^8 the electrons are significantly restrained and the space-charge field in the middle of the avalanche is so increased as to practically cancel out the applied field. The neighbouring field around the avalanche is modified as though by a dipole. In the reduced field in the centre of the charge cloud the electrons are cooled and radiative recombination may

occur within the avalanche,

$$A^+ + e^- \longrightarrow A^* + h\nu$$

isotropically emitting ultraviolet photons which may ionise hydrocarbon molecules outside the space charge cloud, a process which is energetically favoured over ionisation of the argon. Some of the electrons produced in this way may drift back and multiply at the tip of the positive cone where the field is highest. The streamer grows in this way and advances towards the electrodes. On arrival the electrodes become connected by a low resistance conducting plasma of electrons and positive ions, and a current flows between them.

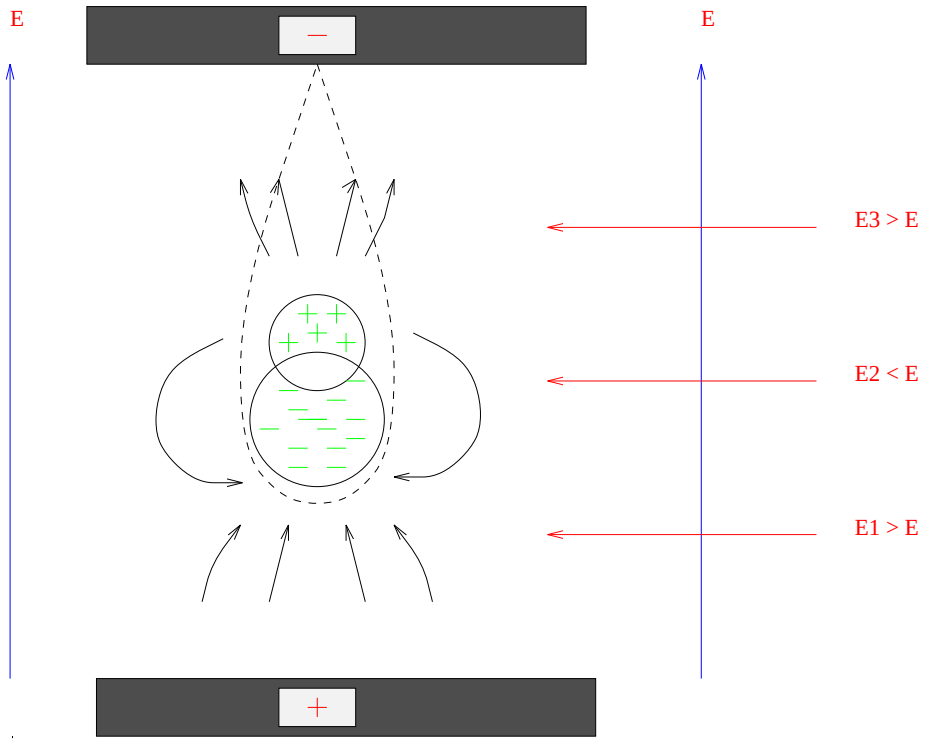

Figure 2.6: Streamer development.

This theory provides an explanation for the triggering of the transition to the streamer, and for the lack of intermediate sizes of pulse. The chance of further

avalanches occurring is small unless the number of recombination photons is large.

An alternative scenario [12] concerns the formation of new avalanches. The ion-pairs created in front of the leading edge of the avalanche and behind the tail of the initial avalanche find themselves in an enhanced electric field, while those to the side experience a reduced field. As a result, those electrons before and behind will accelerate quickly - since α depends on E - and possibly form new avalanches. These grow until they too become large enough to repeat the process. The old and new avalanches merge together to form the streamer, whose ends advance towards the anode and cathode.

The charge deposited on the electrodes is gradually absorbed into the surrounding plate. The time taken for this to happen, and hence for the electric field in the immediate area of the discharge to return to its applied value, is the recovery time for the RPC. The small spatial spread and duration of the streamers and avalanches and the high resistivity of the electrode plates themselves mean that only a very small area around the discharge is affected. The area of the dead zone S can be estimated by approximating the RPC to a perfect parallel plate capacitor: i.e. $S = \frac{Q}{\epsilon_0 E}$ where Q is the average charge generated in the ionisation process and E is the applied electric field. This gives an area of $S \sim 5$ mm^2 - so that the volume fraction of the RPC made inactive by a single ionising particle is negligible, provided the recovery time is sufficiently small.

The recovery time of the chamber can be shown to be

$$\tau = RC = \rho \epsilon \epsilon_0$$

Taking a typical bakelite resistivity of $\rho = 10^{11}$ Ω cm, and $\epsilon \simeq 26.2$ pF m^{-1} [15], gives a value of $\tau \sim 20$ ms. This is much greater than the discharge time of ~ 10 ns, so that with these assumptions the electrodes can be considered as insulators during this process.

This approach leads to the conclusion that the dead time incurred for incident rates such as the normal rate of cosmics should be negligible - and indeed this appears to be so, although as the voltage across the plates is increased the amount of charge carried in the streamers increases and so leads to an increase in the size of the dead zone, which may be a contributing factor to the observed fall-off of efficiency with increasing voltage.

A more thorough approach to this calculation would include consideration of the movement of charge between the inside and outside surfaces of the resistive plates themselves - the deposited charge does not sit on the surface of the plate as in the classical parallel plate capacitor but migrates through it.

2.3 Choice of gas

The main constituent must be a gas which forms avalanches easily: argon is an almost ideal choice for this, since avalanche multiplication occurs at lower electric field values in noble gases than in other gases and argon is far cheaper and more readily available than its counterparts krypton and xenon.

Further gases are needed as quenchers to prevent the chamber going into continuous discharge - since in a pure argon atmosphere spare photoelectrons from the radiative decay of excited gas atoms and spare electrons escaping from the main avalanche can both lead to the development of secondary avalanches. These can then become self-sustaining. Complex polyatomic molecules such as isobutane have many rotational and vibrational excited states, and hence can be used to absorb photons emitted by the deexcitation process in order to inhibit streamer formation. They absorb photons over a wide energy range, and then dissipate the energy through radiationless interactions and dissociation, and without recourse to ionisation. A highly electronegative gas, such as freon, is needed to clear up peripheral electrons around the main body of the avalanche and so reduce the lateral spread of the discharge. This helps to minimise the area of electrode deadened should

the avalanche propagate to form a streamer.

Addition of these types of gases significantly increases the rate capability of the chamber, although unfortunately they are not ideal for work in enclosed spaces, since isobutane is highly flammable, and freon highly environmentally-unfriendly. Work is in progress by other groups to find viable alternatives to isobutane and freon which demonstrate a similarly high efficiency: few results have been published as yet, but mixtures involving the use of carbon tetrafluoride and carbon dioxide in place of freon and $\sim 11\%$ isobutane seem to perform adequately [16].

The gas mixture used in the work for this thesis consisted of: 66% argon, 30% isobutane, 4% freon[2]; these specific proportions were chosen following measurements of RPC performance with different mixtures made during previous research at Manchester [17, 18].

[2]freon 13B1, that is, monobromotrifluoromethane.

Chapter 3

Experimental arrangement

Several bakelite RPCs with different widths of gas gap were used. All had the same sensitive area of 10×10 cm^2 - relatively small compared with commercially-produced chambers - and bakelite plates of about 2mm thickness, with a resistivity of $\simeq 10^{10}$ Ω cm. The chambers had single undivided copper pickup pads, so that no testing of the spatial resolution could be carried out; work concentrated on the timing characteristics and pulse shapes. The gas supply was monitored by a Gossen digital flow meter [19] ; the flow rate was 75 cc/min and the mixture used was the same for all the chambers tested. Voltages below 10kV were supplied by a Bertan 10 kV high voltage supply [21], and those above 10kV by one of two Brandenburg 15kV high voltage supplies [22]. Standard LeCroy quad discrimination and coincidence units [20] were used for basic threshold operations. Any necessary amplification or attenuation was performed using a LeCroy linear fan out and standard amplifier and attenuator units [23].

The chambers were positioned within a scintillator telescope (see fig 3.1 and fig 3.2), consisting of a stack of three scintillators of varying dimensions. The overlapping area of the telescope was approximately 6×6 cm^2, which covered the centre of the active area of the chambers, and was used to establish when a cosmic ray had passed through. The lowest scintillator was shielded from the others and from the surroundings by strategically placed lead bricks to ensure that only incident

particles of high energies would produce a signal. Chambers being tested were placed between the upper two scintillators.

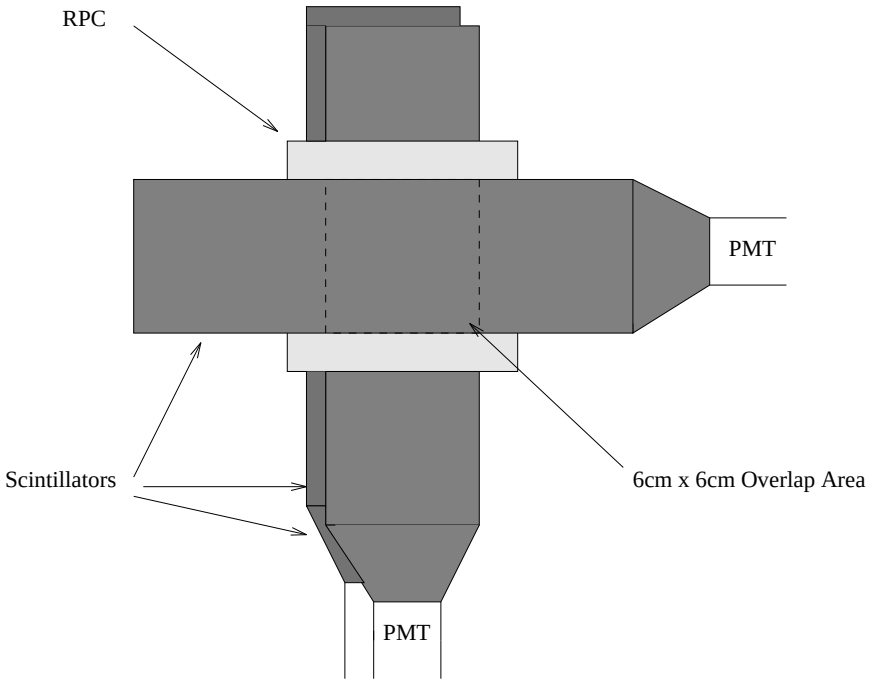

Figure 3.1: Scintillator setup - offset plan view

Due to the intrinsic noise rate of most scintillators - from thermal emission from the photocathode and occasional electrons being produced by radioactive elements within the glass of the light-guide - at least two are needed for a reliable indication of a cosmic ray incidence. In this project three scintillators were used to give a reliable trigger signal: a discriminated signal from each was fed into a coincidence circuit, so that only if all of them gave a pulse would a cosmic be assumed to have passed through the apparatus. The use of three scintillators rather than two was deemed to have a distinct advantage in that there was a much reduced likelihood of random overlap of signals at higher voltages where the coincidence curve between two scintillators tended to begin to climb again off the plateau. The lengths of cable between the photomultiplier tube and the discriminator were the same for

each scintillator output, so that it was not necessary to look at the timing curves for different pairings of scintillator outputs in order to bring them into coincidence.

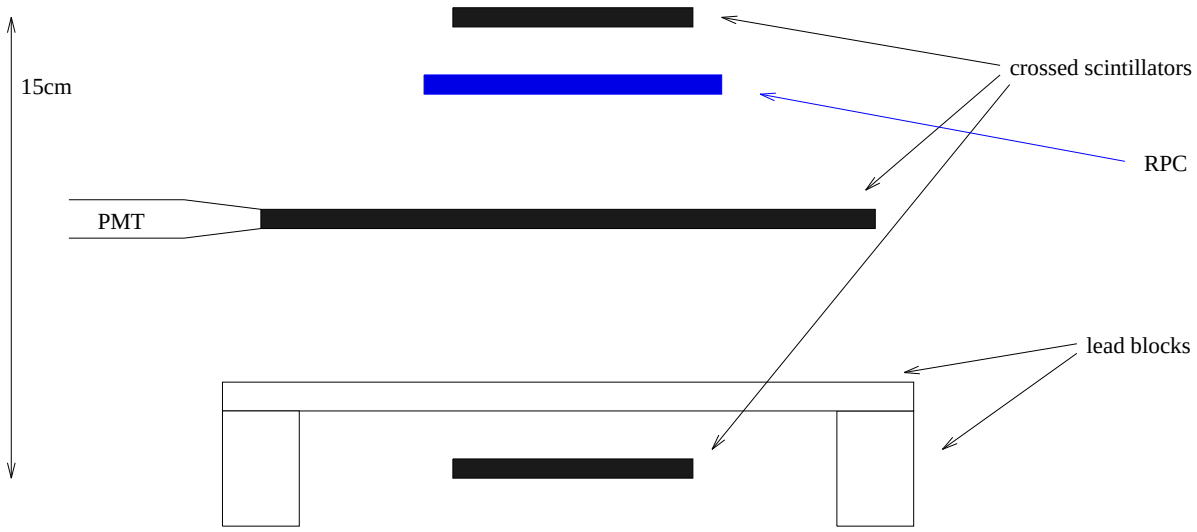

Figure 3.2: Scintillator setup - side view

In order to find the optimum operating voltage of each scintillator, two of them were set at arbitrary voltages within the usual operating range of such counters and the measurements were taken of the coincidence rate between the three as the voltage on the third was varied between 1-2 kV. The coincidence rate rises initially as the efficiency of the photomultiplier tube increases and eventually reaches a plateau at the true coincidence rate beyond which further rises in count rate are due to random coincidences between different counters. The ideal operating voltage for the scintillator is about 100 V into this plateau. The relevant scintillator is then held at this voltage, and the process repeated in turn for the other two. The rate of random coincidences can be estimated using the expression for random overlap of two discriminated scintillator pulses :

$$R_{random} = R_1 \; R_2 \; \tau$$

where τ is the width of the discriminator pulse, and $R_{1,2}$ are the individual singles

rates. Extending this to the coincidence between three pulses leads to the expression:

$$R_{random} \approx R_1 \; R_2 \; R_3 \; \tau^2$$

Taking $\tau = 50$ns and a maximum singles rates of approximately 18 Hz this leads to an estimate of the probable random rate of overlap to be $\leq 3 \times 10^{-11}$. From this it can be seen that the likelihood of noise signals from the three scintillators overlapping randomly is vanishingly small for the operating voltages chosen.

The presence of some RPC detecting volume outside the scintillator telescope might lead to an overestimation of the efficiency of the RPC, should random overlap occur between a coincidence signal from the telescope and a noise pulse from the RPC; but this was considered to be very unlikely and disregarded. The incident rate of hard cosmic rays from above through unit horizontal area is 1.3×10^2 m^{-2} s^{-1} [15]. Taking the overlap of the scintillators to be 6×6 cm^2, this gives an estimate of ~ 28 cosmics per minute.

The rate of coincidences achieved on plateauing of the scintillators was ~ 12 min^{-1}, which agrees reasonably well with the predicted value.

Chapter 4

Efficiency Measurements

4.1 Original chamber

Initially tests were carried out on a bakelite RPC with a 2mm gas gap, whose efficiency as a function of voltage was measured. The overall efficiency was taken to be the ratio of the number of cosmics detected by the chamber in coincidence with the scintillator telescope to those detected by the telescope alone.

Two discriminator circuits with different thresholds were used so that measurements could be made of the proportion of streamer to avalanche pulses produced:

- in order to count the avalanche pulses a preamplification of $\times 16$ and a discriminator threshold [24] at 20 mV were used, and
- to count streamer pulses no amplification and a threshold of 50 mV were used.

(see fig 4.1).

For each reading, the voltage was changed by 25 V and the chamber left for 15 min to stabilise. Counts were taken over runs of about an hour of the numbers of avalanche and streamer pulses and the total number of triggers in that time. Readings were generally taken over about 550-650 triggers.

A graph of the efficiency for any kind of pulse is shown in fig 4.2, which also shows the efficiency for streamer pulses only.

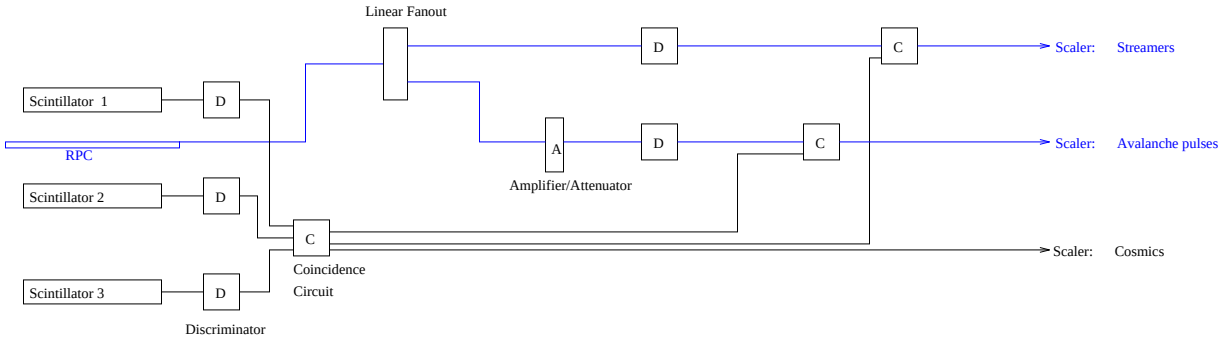

Figure 4.1: Circuit diagram

This graph shows a gradual increase in the efficiency for any pulse with voltage up to a maximum efficiency of $\sim$ 93%. The efficiency reaches a plateau which continues over about 1 kV, and then begins to fall off. This behaviour is consistent with that reported for RPCs in the literature.

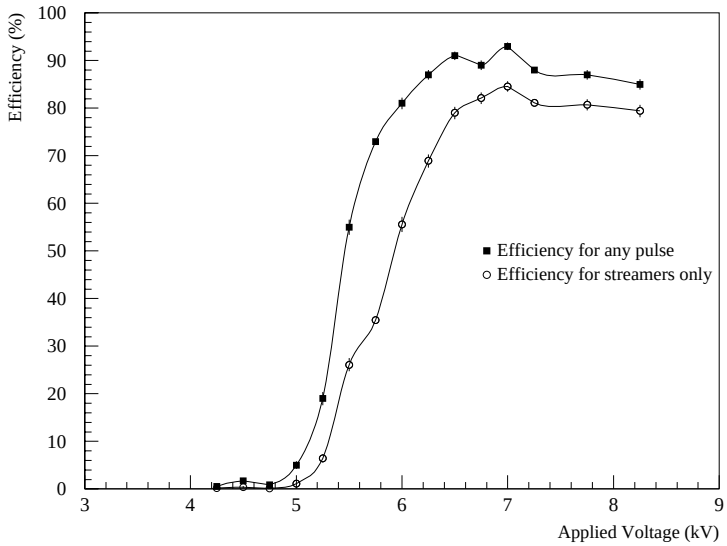

Figure 4.2: Efficiency curve.

Also, the chamber was set at an intermediate voltage (7.00 kV) and succes-

sive measurements of its efficiency were taken over a period of a few days in order to check that the efficiency was not time-dependent and that there were no effects due to, for instance, the building up of charge on the plates. The resulting graph (see fig 4.3) showed variations of the order of a few % for runs of $\sim$ 600 triggers: when the fluctuations in the ambient air pressure over the relevant time period are taken into account these variations appear negligible. The errors shown are the statistical errors calculated for each point.

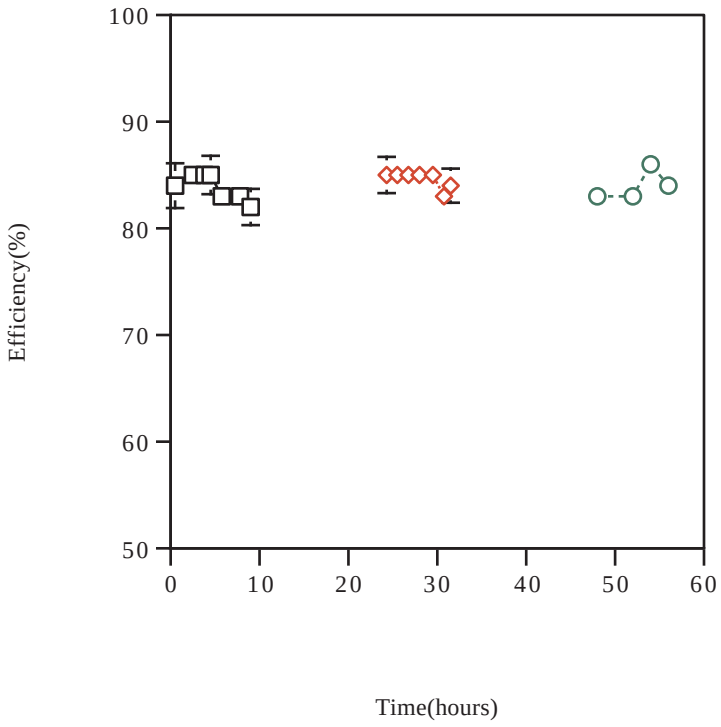

Figure 4.3: Time dependence of efficiency

4.2 Further chambers

At this point three new chambers with gas gaps of 2, 3 and 4 mm respectively and all other characteristics identical (inasmuch as that was possible) were

made in order to investigate the effect of different gap distances, and the original RPC was put aside. The same thresholding as before was used to determine streamers and avalanche pulses and the three were run in parallel so that they experienced the same temperatures and atmospheric pressures. Efficiency measurements were carried out on these chambers as well: the corresponding curve is shown for the 3mm chamber in fig. 4.4, for the 4mm chamber in fig 4.5, and for all three chambers in fig. 4.6.

The 2mm chamber breaks down before it reaches a significant efficiency. The electric field at which it started to draw a sufficiently large current for operation to be impaired seems to correspond to the point at which the onset of streamer activity might be expected. The premature breakdown may have been due to voltage leakage around the sides of the chamber, which only became important at high voltage.

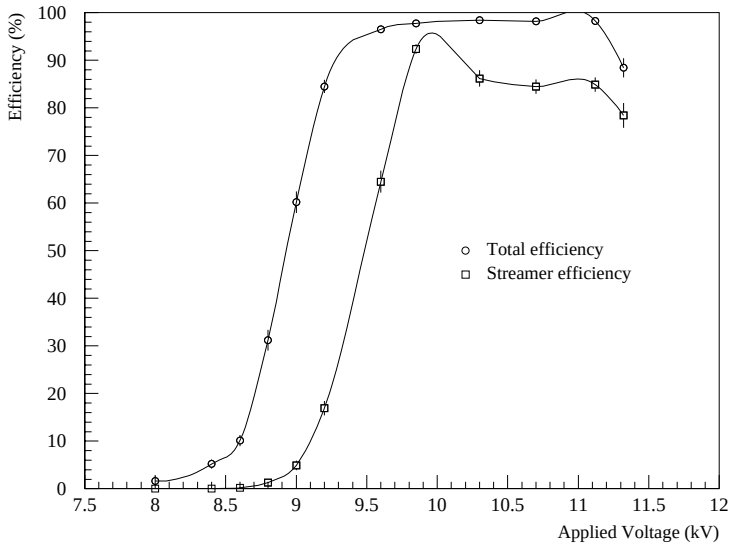

Figure 4.4: Efficiency curve for 3mm RPC.

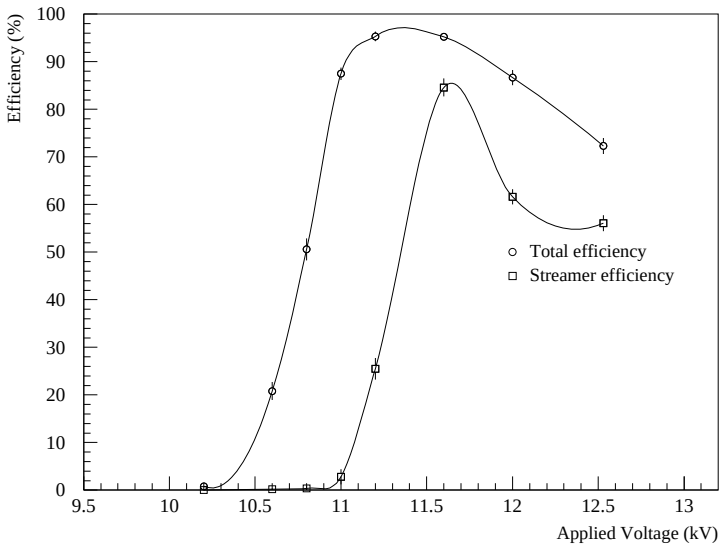

Figure 4.5: Efficiency curve for 4mm RPC.

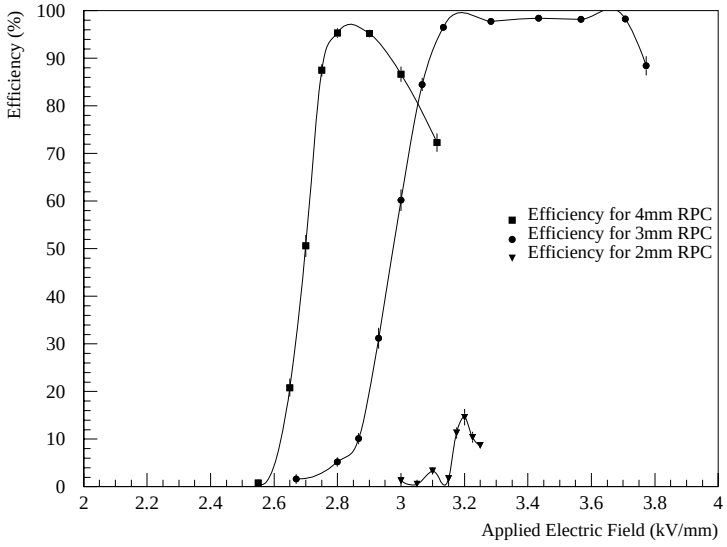

Figure 4.6: Efficiency curves for 2mm, 3mm and 4mm RPCs as a function of the electric field

The efficiencies for the 3mm and 4mm chambers reach acceptably high values when they plateau, but then begin to fall off with increasing voltage again. The plateaus are of the order of 1000 V wide. The fall-off of efficiency has no satisfactory explanation in the literature, but it is often assumed that this occurs as a result of the huge amount of charge carried in the increasingly large streamers leaving a significantly wider area of the plates deadened so that subsequent particles may be missed. However this affect is also observed in RPCs operating solely in the avalanche mode [16], so it would appear that more work needs to be done to explain it.

Figures 4.4 and 4.5 also show the efficiency for streamer pulses only, and demonstrate that, as expected, a higher electric field is required before streamer pulses begin to be formed than that necessary for the production of avalanche pulses. The pulses produced always contain some avalanche pulses and never consist completely of streamers. The curves demonstrating the streamer efficiency begin to fall off at about the same voltages as the curves showing the respective total efficiencies; this is compatible with the idea that, as the streamers become bigger and occur more frequently (since as the voltage is increased more and more of the background, self-triggered, pulses are streamers rather than avalanches), larger areas of the plates are deadened for a larger amount of time and so some pulses are missed.

It should also be noted that the 3mm and 4mm chambers plateau at different values of the applied electric field. From the simple mechanism for streamer formation described in chapter 2 it seems that the most important contributing factor in this mechanism is the value of the applied electric field, so that readings showing streamer formation starting at different fields for different gap sizes seems to demonstrate that other parameters need to be taken into consideration. However, a wider gas gap has a larger volume of gas in which the original ionising particle interacts, so that there is a higher probability of an interaction occurring in a larger gas gap than a smaller one if both have the same value of applied electric field. Hence, it is more likely for an avalanche to be formed in a larger gap at a lower

field than in a smaller gap; and consequently there will be a greater probability of a streamer forming at such a field in a wider gap than in a narrower one.

An empirically determined straight line has been shown in [16] relating the size of gap of a chamber to the applied voltage at which it reaches its highest efficiency. The values measured for our RPCs fit onto a similar line parallel to this but displaced upwards - showing that a higher voltage is needed by a Manchester RPC in order to reach its highest efficiency. This is presumably an effect of the different gas mixtures under use.

Chapter 5

Test beam work at CERN

Two RPCs - one with a 3mm gas gap, and a newly built chamber with a 5.8 mm gas gap - were taken out to CERN for a test beam run with part of the LAA[1] group who are also working on RPCs and their applications in future experiments. It was hoped that information about the behaviour of the Manchester chambers under varying rates of incident particles could be measured, and hence deductions made about the suitability of bakelite RPCs for use in detectors operating under high rates.

5.1 Tests in the laboratory

The variation of the efficiency of the chambers with high voltage was tested in a lab on the CERN site, using the gas mixture that the LAA group customarily used in their melamine RPCs, ie: 78 % argon, 11 % isobutane, 7% carbon tetrafluoride, 3% carbon dioxide, and a small amount ($\sim$ 1%) of water vapour. Studies done by the group on the effect of a dry gas supply on the resistivity of their melamine chambers and hence on their efficiencies [16], have shown that the constant feed-through of a dry gas tends to leach essential water out of the plastic plates and leads to unpredictable changes in resistivity and premature ageing: a small percent-

[1]Lepton Asymmetry Analyser

age of water vapour is included in the gas mixture in order to combat this effect. Bakelite chambers made by industry customarily have a layer of linseed oil on the inside which would help to prevent this kind of water loss; the Manchester chambers do not, and this may be another factor contributing to the slight tendency of the chamber behaviour to fluctuate with the weather. Carbon tetrafluoride is highly electronegative and was included as a quencher, fulfilling the same role as freon in our original gas mixture. Freon however is an extremely non-ozone-friendly gas and its use is being phased out, whereas carbon tetrafluoride - although less effective as a quencher - is a much safer and more environment-friendly gas and so is more suitable for use in a future experiment. The carbon dioxide is added to the mixture as another quencher to further reduce the probability of streamers occurring, the aim being to operate the melamine chambers in avalanche mode only.

The electronics setup involved a standard cosmic ray trigger, with a $\times 10$ amplifier and 30mV discriminator: similar to the arrangement in the lab in Manchester except for the lower level of amplification. The results of the tests on the 3mm RPC are summarised in figure 5.1. The response of the chamber flattened out at an efficiency of about 41 % without drawing current, at which point it was decided that the efficiency had plateaued.

Tests performed on the 5.8 mm RPC showed that, despite taking the voltage up to 13.0 kV, only a spurious level of efficiency ($\sim 1-3\%$) consistent with the accidental overlap of noise signals with the cosmic trigger pulse was reached.

The performances were not very impressive; in the case of the 5.8 mm this was blamed on some possible error in fabrication, while in the case of the 3 mm it was thought to be due to the different level of amplification used so that many of the smaller avalanche pulses would be missed.

The 5.8 mm was taken apart and checked before being tested in the beam, and it was decided that the poor efficiency might have been caused by the proximity of the high voltage plane to the signal plane, leading to voltage leakage between the

two. On changing the design so that these planes were on opposite sides of the gas gap, this RPC achieved significantly higher efficiencies than before.

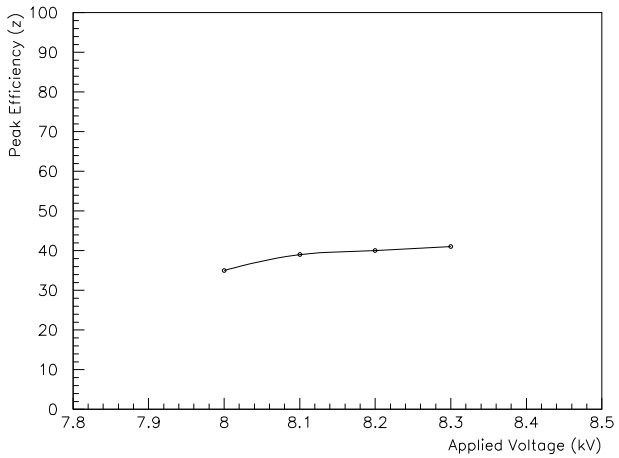

Figure 5.1: Results from testing the 3mm RPC with cosmics in the laboratory.

5.2 Tests in the beam

Tests were carried out in a set up in the East Hall (building 157) at CERN with a defocussed 8 GeV pion beam; the number of particles in each spill was controlled by varying the width of the collimator after the final bending magnet. A coincidence between three scintillators was used for the triggering, the smallest scintillator having an area of 4 cm by 4 cm so that it covered a slightly smaller area than the active area of the RPC. The logic was set up as in the lab and counts were taken of the number of coincidences from the scintillators and the number of these seen by the RPC. Counts for a particular value of incident flux and of applied voltage were generally recorded over three spills - where a spill lasted for 400 ms and arrived every 15 seconds - and the values of flux and efficiency taken as the average over the three readings. In each case the voltage applied across the chamber was varied by about 500 V on either side of the point at which maximum efficiency

was reached, unless the chamber threatened to break down in this region. Repeated readings at the same values of voltage and flux occasionally failed to correspond and wide variations of efficiencies (by $\sim \pm 6\%$) resulted from apparently identical conditions. There was no obvious explanation for this, although at the time it was thought that the effect might be related to irregularities in the surfaces of the plates or to trouble with the gas mixing (given the necessity for the Manchester chambers to adapt and equilibrate to a different gas mixture, and particularly to the water vapour introduced).

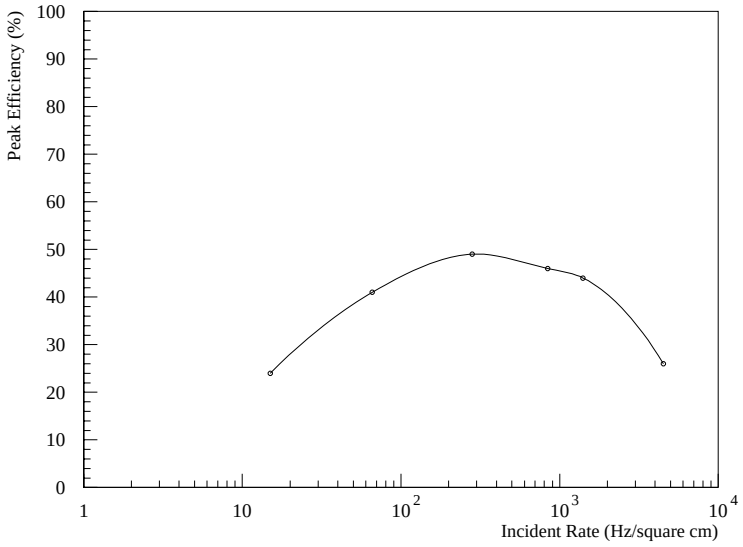

Figure 5.2: Peak efficiency of 3mm chamber in beam.

Figures 5.2 and 5.3 show the maximum efficiencies reached by the chambers after variation of the voltages for each value of the incident flux. Taking into account the variation in some readings taken under the same conditions, statistical errors do not seem meaningfully to represent the uncertainty in the data points, so error bars are not shown.

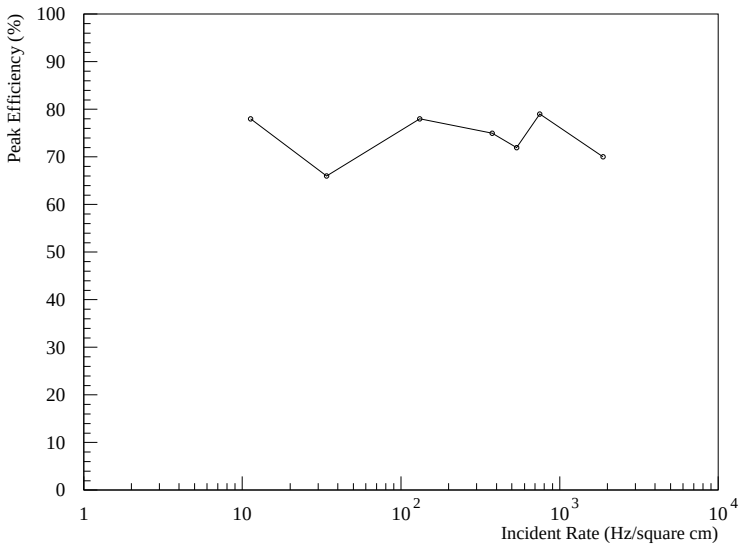

Figure 5.3: Peak efficiency of 5.8mm chamber in beam.

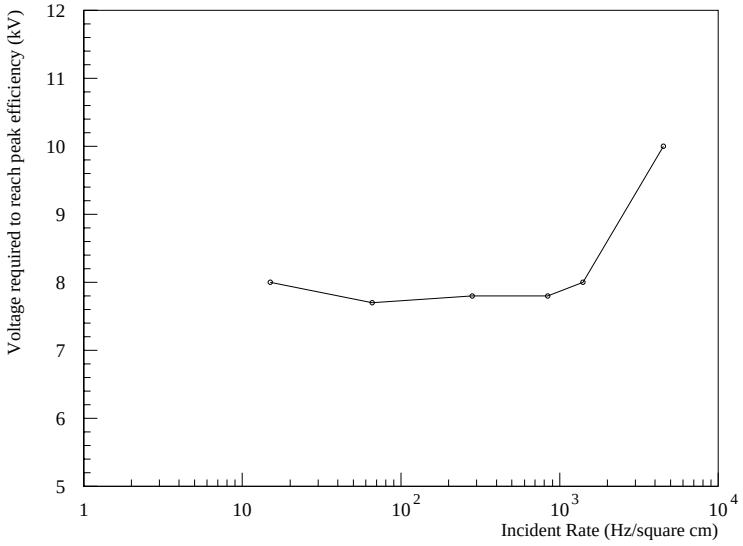

Figure 5.4: The applied voltage necessary for maximum efficiency of the 3mm RPC.

In the RPC literature, measurements have shown a fall in efficiency as the incident flux is increased. For instance, a fall from 97 % to 86 % was measured when the rate was increased from 0 to 100 Hz cm^{-2} by Bertino et al. [27] using RPCs with phenolic plates and irradiating a spot in the centre of a large (2m $\times$ 1m) chamber. Tests performed by irradiating the entire active area of a small phenolic RPC performed by Crotty et al. [28] showed a 45 % drop in efficiency over the same range of flux.[2] With this evidence, it was expected that the Manchester RPCs would achieve a reasonable efficiency at low rate, and that this would gradually tail off as they were subjected to higher and higher fluxes. However, as figures 5.2 and 5.3 show, this was not the behaviour demonstrated.

Much of the behaviour of the 3mm chamber seems consistent with that measured in the lab in Manchester, given the higher threshold being used here for avalanche pulses. Its apparent improvement in efficiency with the incident rate followed by a fall in efficiency with further increasing rate, however, cannot be satisfactorily explained by this different thresholding. The voltage required to reach the maximum efficiency increased from 7.7kV at the lowest incident flux, to 10.0kV at 24000 particles per spill (see fig 5.4).

The 5.8 mm chamber reached an almost acceptably high efficiency, and showed only a small decrease in this up to 8kHz/cm^2. This seemed quite promising, although it would seem more likely that a moderate efficiency would be more possible to sustain than a high one and so this performance might not be continued were the chamber to be operating at a higher efficiency.

[2]The discrepancy between these two results was taken as evidence that the effect of lateral diffusion should be taken into account when testing RPCs.

Chapter 6

Pulse shapes and Pulse-height distributions

On returning to Manchester, work concentrated on the shapes and timing characteristics of the pulses.

Individual pulses could be examined using a Hewlett Packard 250 MHz digitising oscilloscope [25] triggering on the coincidence signal from the scintillators. From this it could be seen that the sizes of the avalanche pulses tended to range from below the noise level ($\simeq$ 1mV) to 5 mV for the 3mm gas gap chamber, and between 1mV to 10 mV for the 4 mm chamber. These pulses arrived consistently earlier than the coincidence trigger by a margin of 10 - 30 ns (depending slightly on the gas gap and on the applied voltage), and had risetimes of about 10 ns.

The avalanche pulses from the 4mm RPC tended to arrive later than those from the 3mm, but were still earlier than the trigger pulse due to delay in the photomultiplier tube. A typical electron transit time for the photomultiplier tubes we were using is up to 40 ns, and all cable lengths were matched to within a couple of nanoseconds, so that this is a fairly reliable indication of the reaction-time of the RPCs with respect to the more conventional PMT technology. The time distributions of avalanche pulses shown in chapter 7 provide further evidence of this.

The streamers were generally of the order of 100 - 200 mV, with risetimes

of about 20 ns. Their time of arrival with respect to the coincidence trigger varied from being equivalent to that of an avalanche pulse under the same conditions to 100 or 200 ns later than the trigger.

6.1 Data acquisition and analysis

Information about the pulses was collected using two 100 MHz FADC F1001 [26] cards connected to a scanner and a Mac running the DL400 [26] Testdaq data acquisition program [29, 30]. The FADCs sample continuously until they receive a stop signal from the scanner - this was provided using a delayed pulse from the coincidence between the three scintillators - at which point the data is frozen in the FADC memories. It remains there until it is copied into the Mac's memory. Figure 6.1 shows the set-up used to read out the signal data. Each chamber used two FADC channels - in general one channel received an amplified signal, and one the unamplified version.

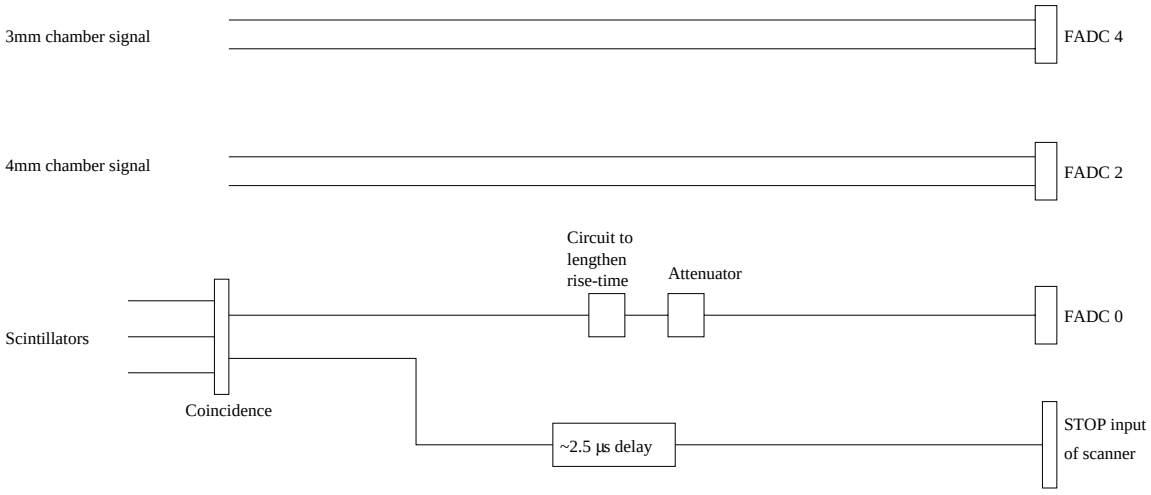

Figure 6.1: Logic diagram for Pulse-Height spectrum analysis.

The risetime of the output pulse from the coincidence unit was increased so that the rising edge was spread over more than one FADC digitisation (see fig.

6.2: this circuit halves the size of the signal and spreads the rising edge over about 4 FADC digitisings). A $\times 0.6$ attenuator was also used in order to reduce the signal size still further so that it did not saturate the FADC. This ensured that the analysis program had more than a single bin from which to extrapolate the arrival time of the pulse, and hence give more accurate time determination.

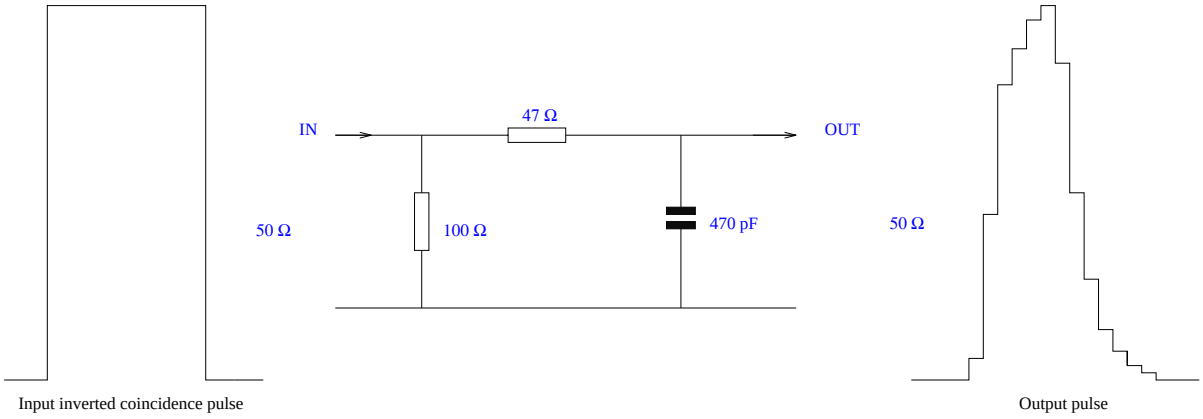

Figure 6.2: RC circuit to slow the risetime of the trigger signal.

The trigger time is taken as the time of any pulse found in the zeroth FADC channel with a height above 80 units and an arrival time between 15 and 75 FADC digitisings.

The data files were transferred from the Mac onto a DEC Alpha, where they were processed by the DCTEST analysis program [31]. This program unpacks the data from the Mac format and then analyses it to find parameters such as drift times, pulse-heights and pedestals, which are fed into an ntuple and analysed in PAW. DCTEST finds the starts of pulses by looking for two successive rising digitisings above threshold. The end of the pulse is allocated after a peak and then two consecutively falling bins below threshold have been found. The time of arrival of each pulse is calculated by extrapolating a straight line through the two most steeply rising digitisings on the leading edge of the pulse down to the pedestal.

Thresholds were found for individual runs of data by using an offshoot of

the DCTEST program which produces an ntuple consisting of a series of histograms of single events as they appear after digitisation, so that the shapes and general appearance of pulses and the background noise can be seen and checked against what is expected. A selection of events in the middle of a run were chosen, and the levels of noise assessed in each case so that suitable thresholds could be set. The values of the thresholds and other parameters such as the differences between the rising/falling digitisings and so on are set in a file which can be edited each time a run of data is analysed by DCTEST.

6.2 Pulse-height spectra

Pulse-height spectra were made using two channels - one with a $\times 10$ preamplifer and one unamplified - for each chamber so that the full range of the pulse sizes could be seen. The height spectra for the initial pulse in any event were plotted in PAW. For multipulsing events (see fig 2.4, c) the heights and times of succeeding pulses after the initial one could also be shown, but the values found for these were slightly unreliable due to the difficulty of establishing a pedestal correctly and also to the reaction of the amplifier to very large pulses.

The pulse height spectra for the amplified (avalanche) and non-amplified (streamer) channels for the 3mm chamber are shown in figures 6.3 and 6.4, and figures 6.5 and 6.6 show the corresponding spectra for the 4mm chamber. The scales on the x-axes correspond to mV on a 50Ω resistance. The data for each graph were taken over the same number of triggers, so that the increasing numbers of hits for each graph correspond well to the gradual rise in efficiency with increasing voltage. The evolution of the spectra with voltage can be clearly seen, as the mean heights of both populations increase significantly over a range of 2 kV. The spread in pulse heights for both avalanche and streamer pulses appears to be approximately the same for both chambers.

The data for the 3mm chamber at 10.4 kV and 10.6 kV were taken at a higher level of attentuation so that fewer pulses would saturate and a more meaningful indication of the spread of pulses could be gained. Because of this, the numbers obtained from analysis of these data are not directly comparable with those for the data taken at lower voltages.

The populations of pulses seem very much as one would expect from either of the theories outlined in chapter 2. The avalanche pulses are small and tend not to grow beyond a certain maximum size; as the applied field is increased, the maximum size to which an avalanche must grow before it overcomes the field sufficiently for radiative recombination to take place increases. The streamers have a minimum size, which also increases as the field is increased. There are occasional pulses of intermediate sizes, but nowhere are these sufficient to form a distinguishable third population.

The spectra support the concept of the two modes of operation with a transition between them, but do not provide much information as to a likely mechanism for this transition.

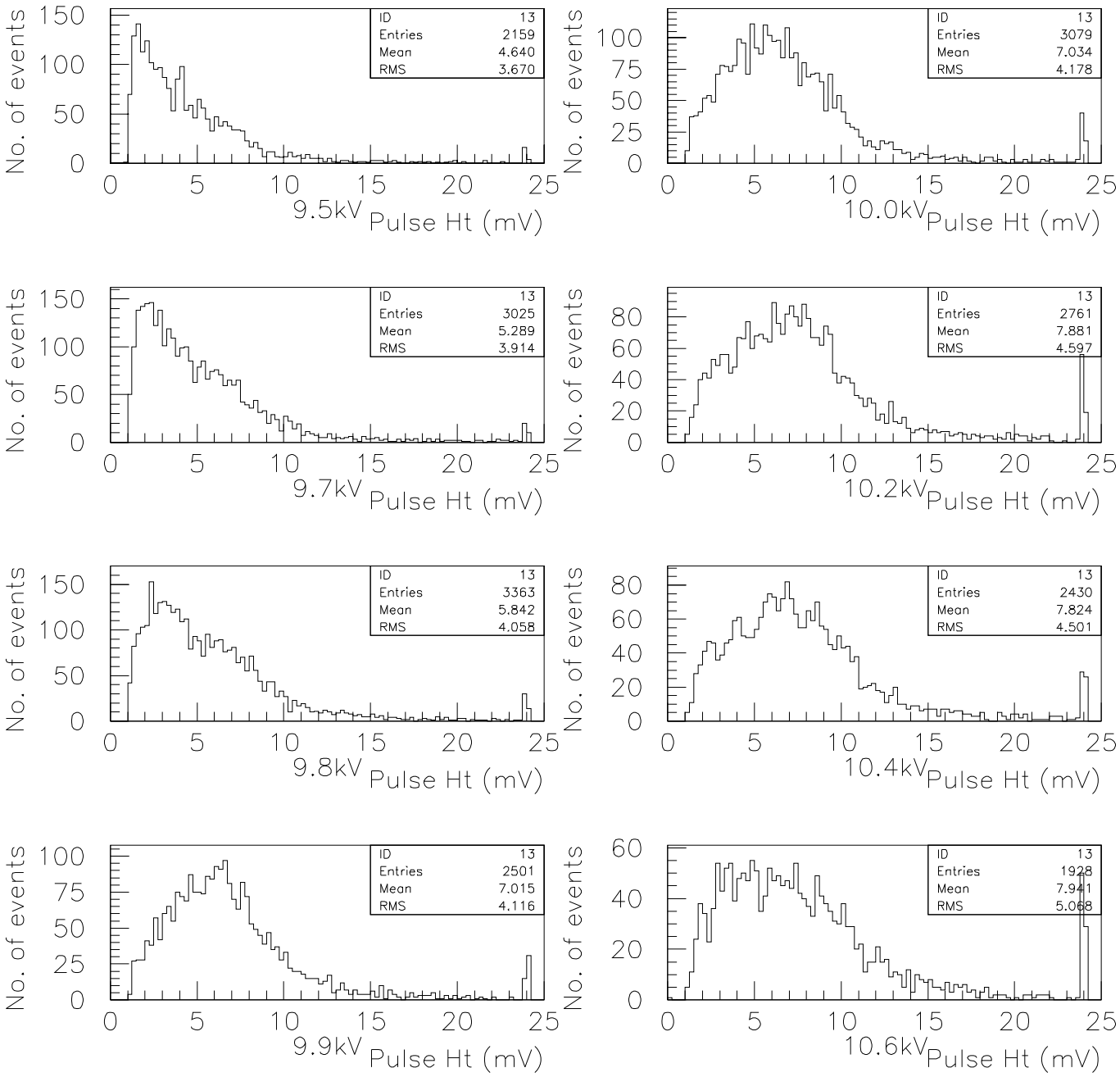

Figure 6.3: Evolution of 3mm avalanche pulse-heights with voltage.

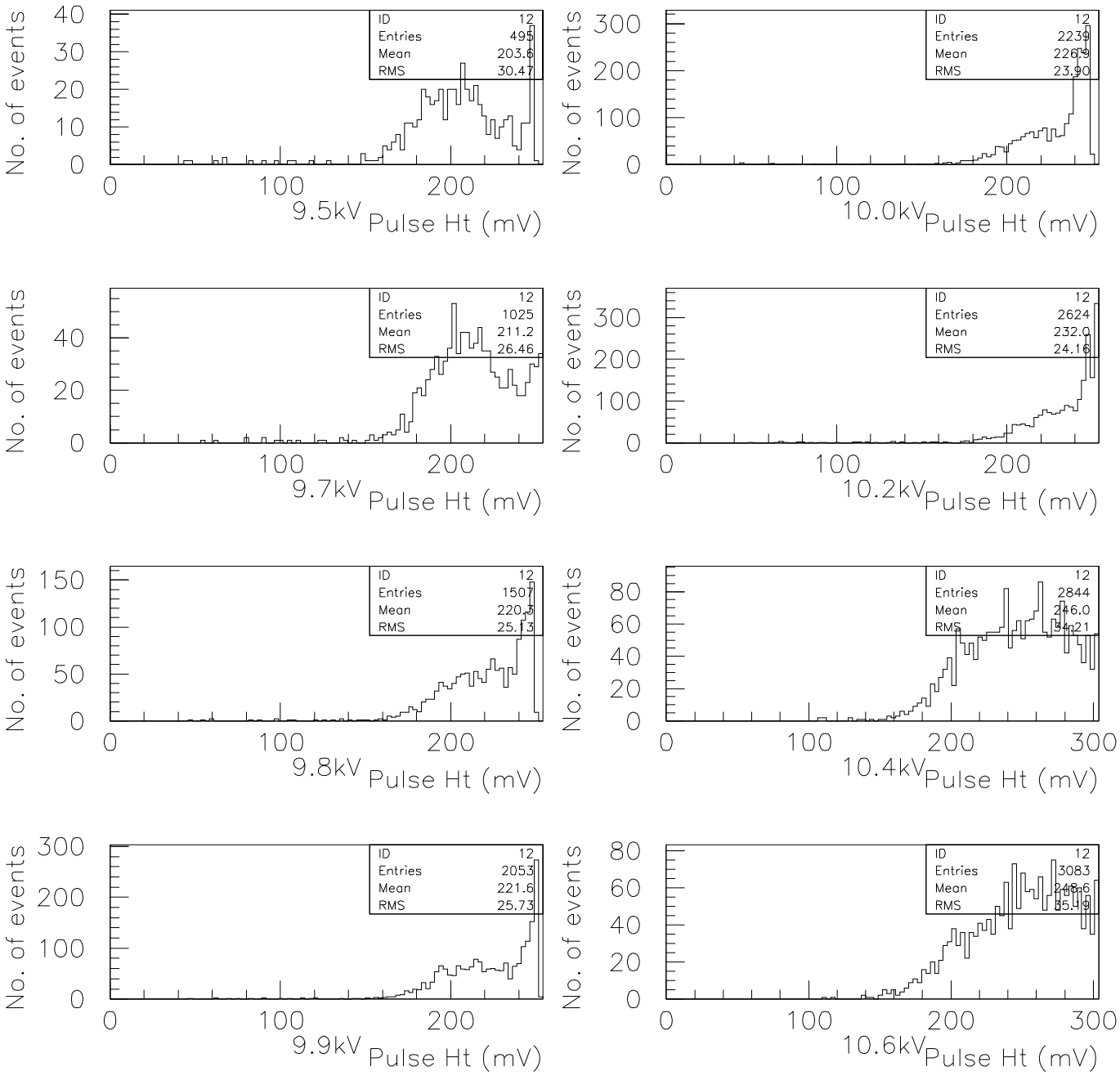

Figure 6.4: Evolution of 3mm streamer pulse-heights with voltage.

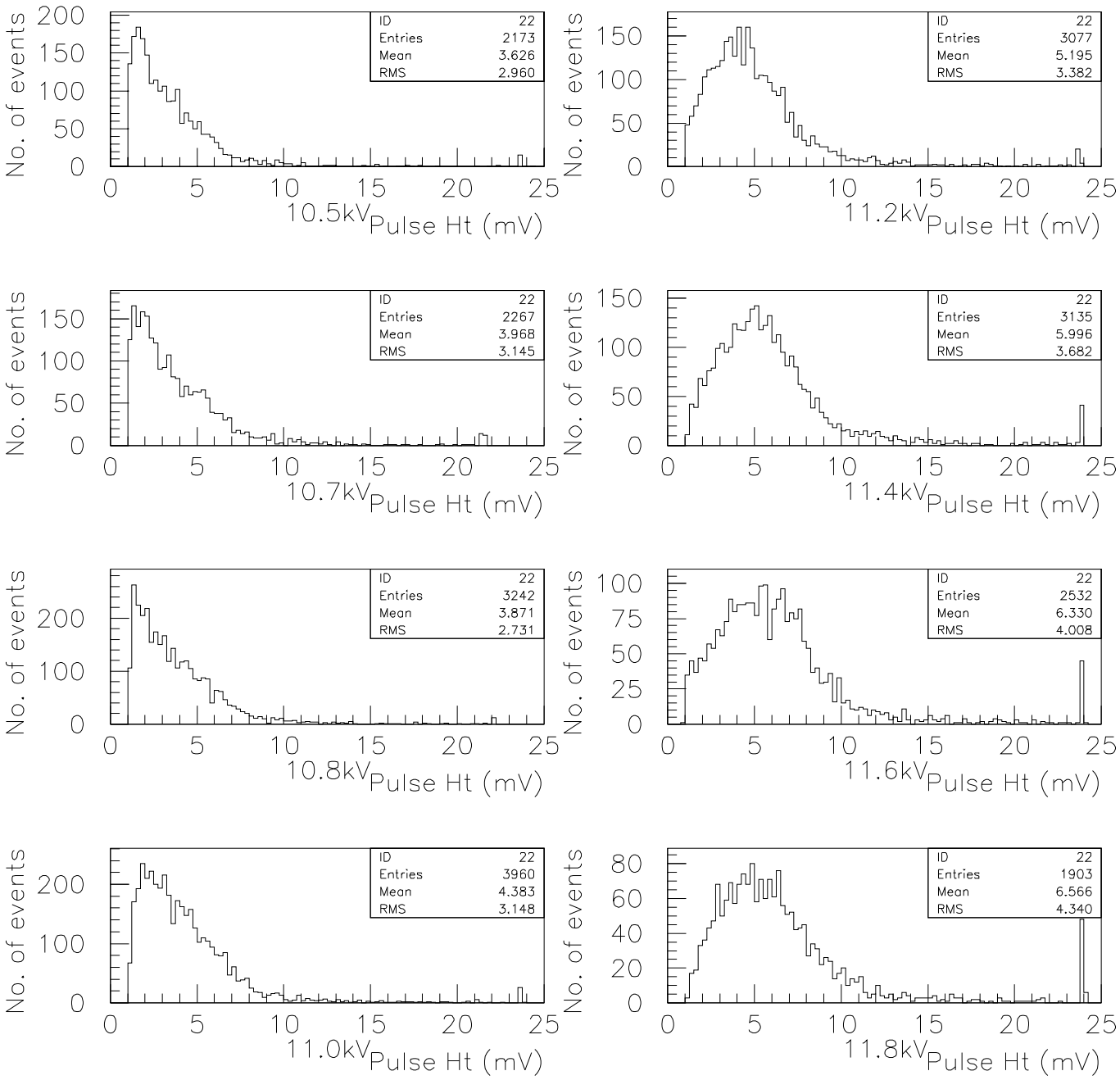

Figure 6.5: Evolution of 4mm avalanche pulse-heights with voltage.

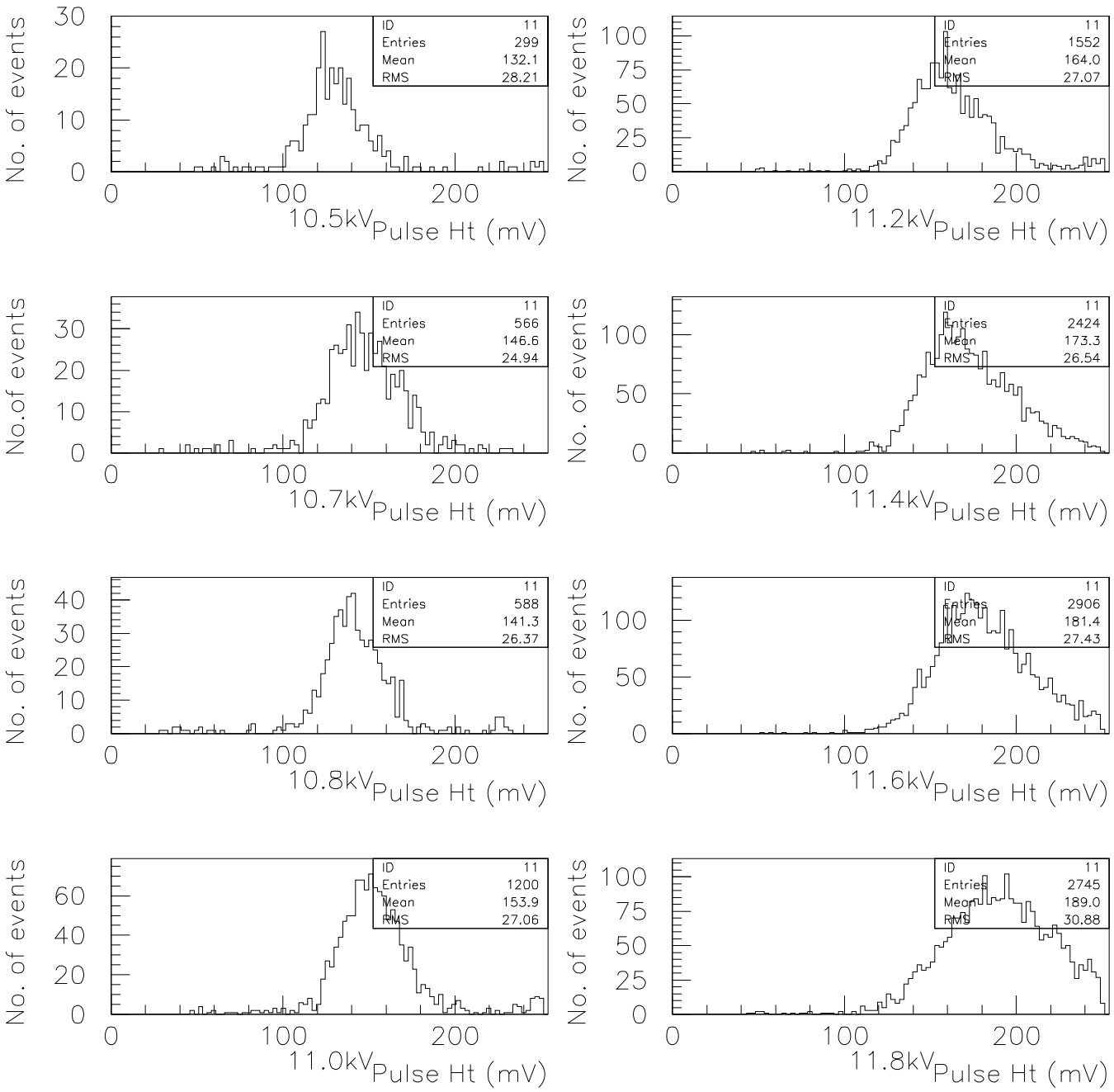

Figure 6.6: Evolution of 4mm streamer pulse-heights with voltage.

6.3 The transition from avalanche to streamer mode

Figures 6.3, 6.4, 6.5, 6.6 also demonstrate the gradual change in the proportion of avalanche to streamer pulses seen as the voltage increases: the number of events **without** a streamer pulse declining as the number of events **with** a streamer increases. This accords well with the theory that there is a transition from avalanche to streamer which becomes more likely as the voltage is raised. To test this more fully the numbers of events which gave rise to an avalanche pulse *only*, and of those which gave a prepulse followed by a streamer pulse, were found for different voltages. Events where a streamer pulse arrived first with no prepulse were assumed to be examples of a very prompt streamer following a prepulse so closely as to submerge it, and so were included in the latter category.

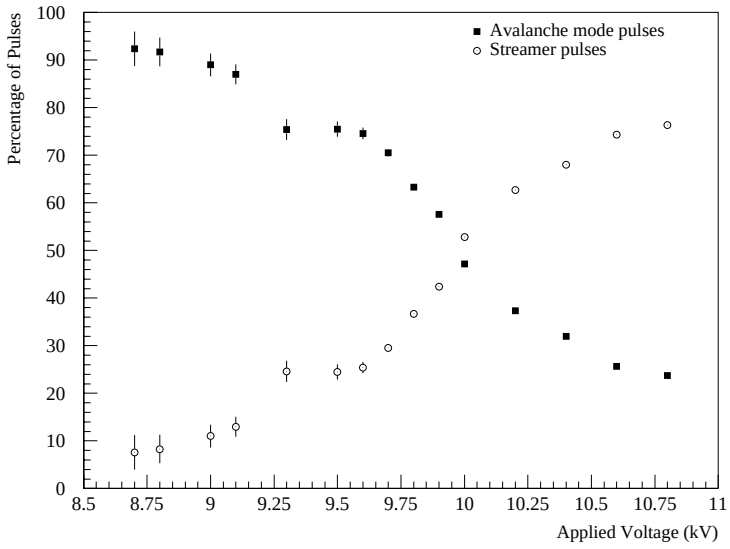

Figure 6.7: Transition from avalanche mode to streamer mode for 3mm chamber.

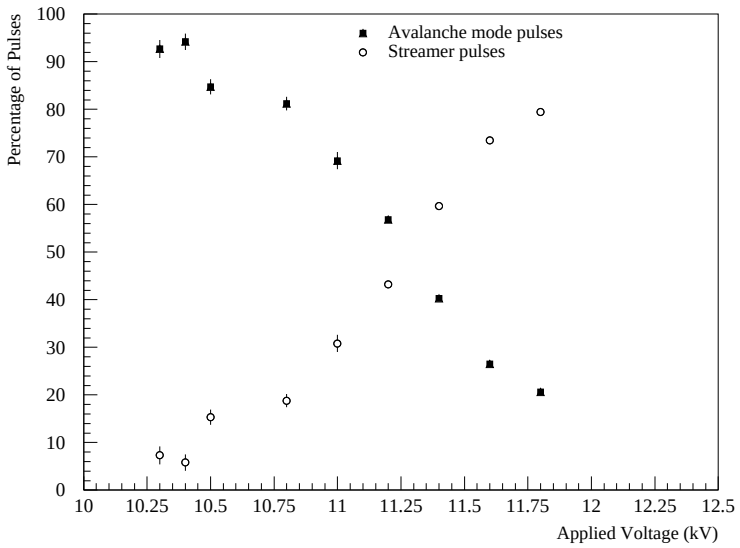

Figure 6.8: Transition from avalanche mode to streamer mode for 4mm chamber.

Figure 6.7 shows the variation of the numbers of pulses falling into each category as a percentage of the total number of pulses seen for the 3mm chamber, and figure 6.8 that for the 4mm chamber. The proportion of events where an avalanche pulse only is seen falls gradually as the voltage is increased, but seems never to reach zero. The graphs show strong evidence for a transition from one type of pulse to the other over a voltage range of several kV, and also present a good case for operation in the avalanche mode, since the streamer efficiency never reaches 100%.

Chapter 7

Timing measurements

7.1 Resolution of the avalanche pulses

The time resolution for the avalanche pulses alone was investigated as a function of the applied voltage. Cuts were used to give a distribution of the time of arrival of the initial pulse with respect to the scintillator trigger in any event with a pulse smaller than 40 mV. Each distribution plotted in this way was fitted with a Gaussian, and the standard deviation of the fitted curve found. The curve fits are shown in figures 7.1 and 7.2. The curves, whilst not being a particularly good fit to the data, are fair representations of the general distributions.

Given that the experimental sampling rate was 100 MHz, a high accuracy was not to be expected: the error on the mean of a Gaussian fitted to the data has a contribution of $\frac{10}{\sqrt{12}} = \pm 2.9$ ns from this factor alone, and then a further uncertainty due to the time-finding algorithm which has been estimated as ± 1.4 ns.

Fig. 7.3 shows the variation in the resolution, fig. 7.4 that of the means, of the distributions with increasing voltage. Both chambers seem to show a general improvement of the resolution with higher field, reaching the best resolution at a value of the field which is about halfway into the efficiency plateau, and then a slight worsening in resolution towards the region where the efficiency begins to fall off. The means show a trend towards pulses arriving earlier as the voltage is increased.

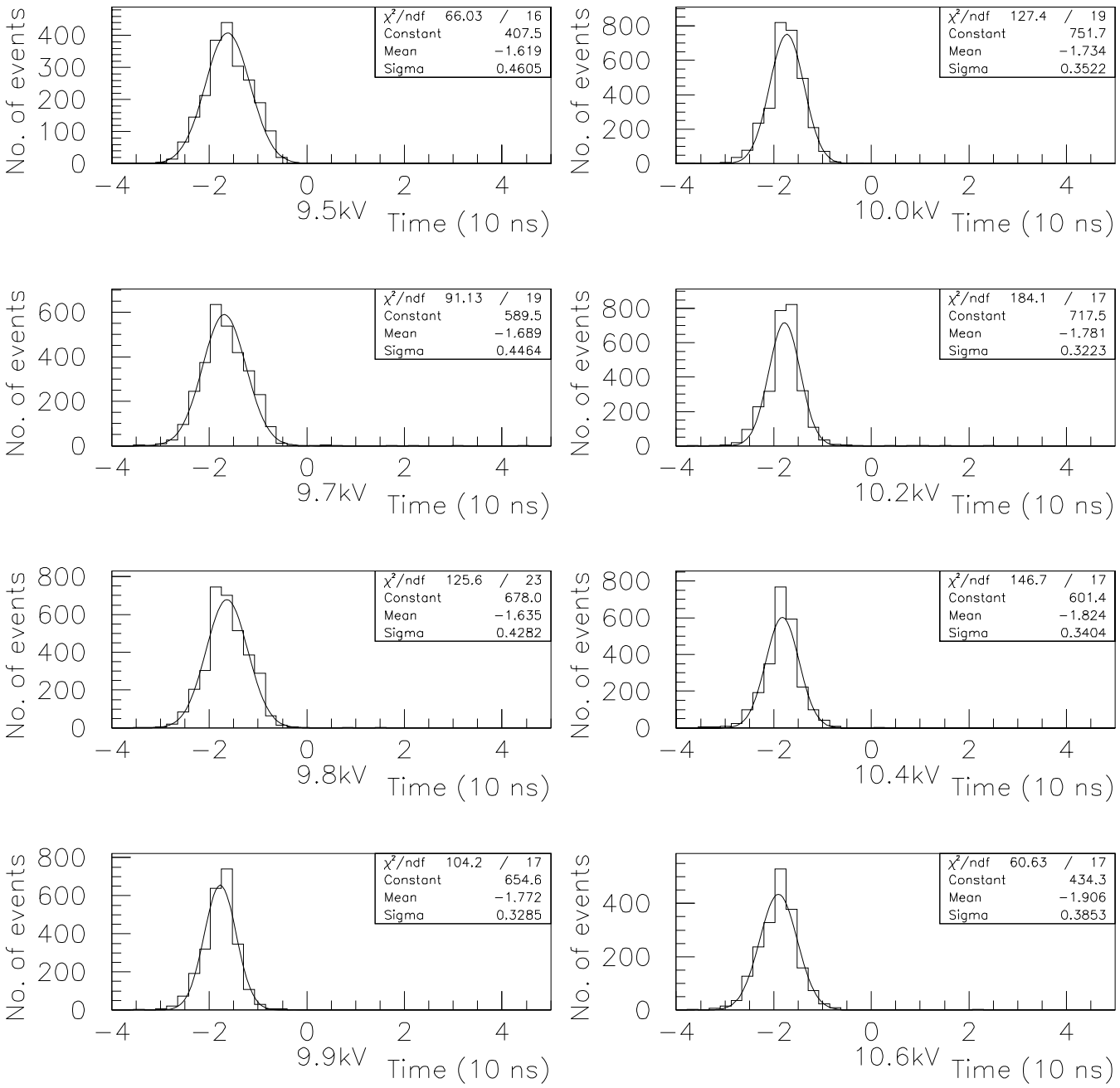

Figure 7.1: Timing resolutions for 3mm avalanche pulses, as a function of voltage.

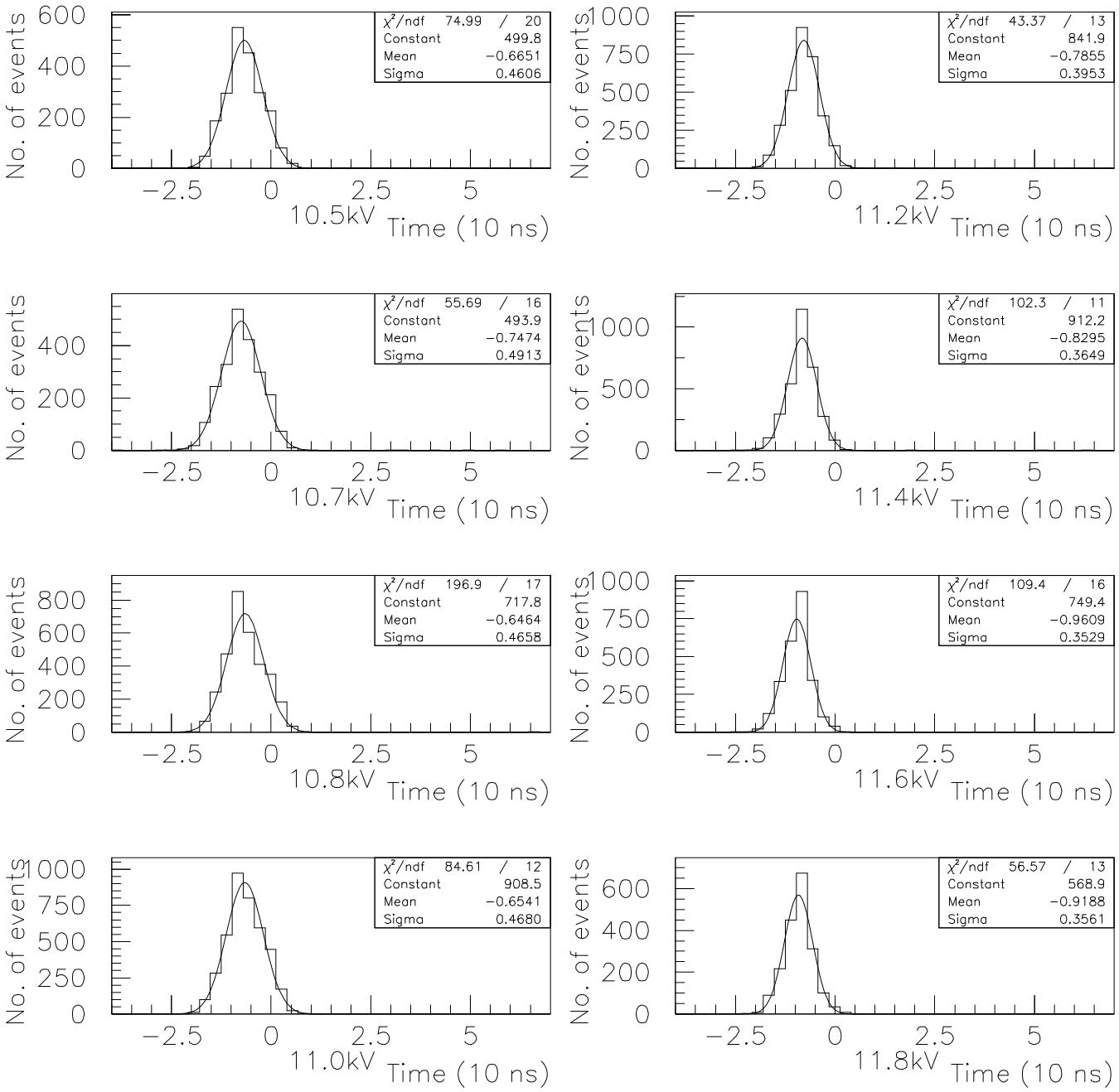

Figure 7.2: Timing resolutions for 4mm avalanche pulses, as a function of voltage.

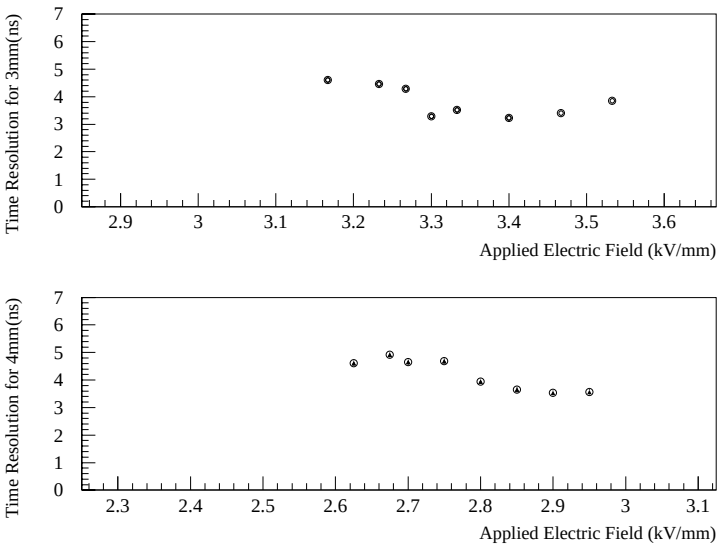

Figure 7.3: Variation in timing resolution with voltage for 3mm and 4mm RPCs.

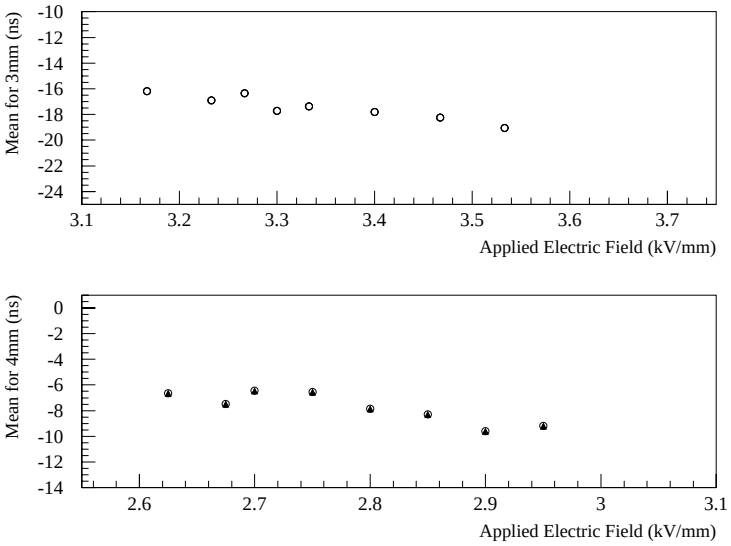

Figure 7.4: Variation in timing mean with voltage for 3mm and 4mm RPCs.

7.2 Modification of the DCTEST program

One of the more interesting and informative factors in attempting to determine a mechanism for the streamer formation seemed to be the variable time gap between a streamer and the prepulse it followed (see, for example, fig 7.6). Given the assumption that a prompt streamer overlaid its prepulse, so that the time difference for such an event was zero, the time differences varied from zero to several hundred nanoseconds. In order to obtain distributions of these time differences for a range of voltages, it was necessary to modify the analysis program being used.

DCTEST was a test program originally written to analyse pulses detected on drift chamber wires, and so had to be modified in order to investigate single-ended pulses. Each FADC has four inputs: the analysis program divides these four into two pairs and treats each one of a pair as either end of a wire. Pulses found in both channels of a pair are treated as the same pulse arriving at the two ends of a sense wire if the times of arrival in each channel are within 40 ns of each other. In this way it was possible to study both the very small and very large types of pulse at the same time - an amplified signal was fed into one channel and an unamplified signal into the other. The cable delays and times taken for passing through the amplifiers were matched for each channel so that the pulses would arrive at the FADCs at the same time relative to one another as they were picked up from the chamber.

The DCTEST program is written in such a way that the first parameter calculated is the trigger time - i.e. the time of arrival of a pulse in the zeroth FADC channel which satisfies all the stipulated requirements to be a trigger pulse. This time is then set as the trigger time `t01` for all the data channels. In the analysis of the data, the next parameter calculated is the number of hits in each channel for a particular trigger. A loop is then entered in which other variables such as drift times, pedestals, heights and so on, are calculated for the first hit in the first data channel (FADC2 end 0), and then the others sequentially until it reaches the last. It then returns to the start of the loop and calculates the same variables for the *second*

hit found for each channel in order, (see fig 7.5). Table 7.1 shows the parameters calculated for each pulse which were used. The FADCs work at a sampling frequency of 100MHz, so that an FADC time bin is 10ns wide, hence all timing plots are to a $\times 10$ ns scale.

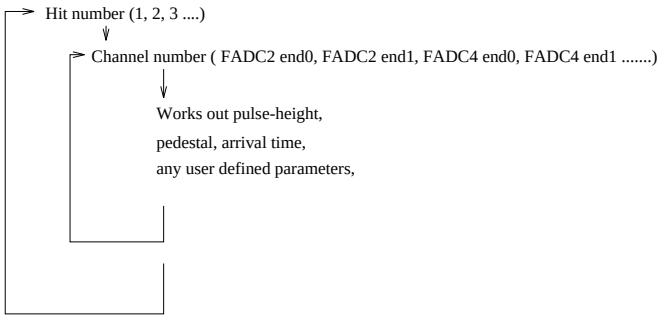

Figure 7.5: DCTEST parameter calculation loop logic.

The code was written in such a way that it was not possible to plot graphs of the times of arrival of more than one pulse in the same event, for instance the time of the first pulse could be plotted, but not on the same graph as that of the second. This made it necessary to modify the DCTEST code in order to be able to find the time of arrival of a large pulse which had been preceded by a small prepulse. Some code was written in the part of the logic loop where the standard parameters were calculated, so that the times for the particular pulse configuration of interest would be found and included in the output ntuple.

This new code introduced two new parameters:

- the time of arrival of a small pulse being detected as the first pulse in an event, and
- the time of arrival of a large pulse *following such a small pulse.*

A small pulse was defined as a pulse found in the amplified channel which did not saturate and which had an integrated charge[1] in that channel of less than

[1]The integrated charge is set to zero if a pulse saturates the FADC.

xTuple number	Name	
xTuple(4)	`ihit`	Number of the hit found
xTuple(5)	`fadc`	FADC number
xTuple(6)	`t`	Time of arrival (with respect to the
		trigger pulse) of the pulse averaged
		between the two channels in the pair
xTuple(7)	`td`	Time difference between the arrival
		times in the two channels
xTuple(8)	`q1`	Integrated charge found for the
		pulse in the unamplified channel
xTuple(9)	`q2`	Integrated charge found for the
		pulse in the amplified channel
xTuple(13)	`t01`	Time of arrival of the trigger pulse

Table 7.1: Table showing the xTuple members used.

200 units. The time was taken as the time of arrival measured in the amplified channel.

The time was found for a streamer following such a pulse (should all the conditions above be satisfied) by then requiring a pulse to be found in the non-amplified channel. The time for this case was taken as the time of arrival measured in the non-amplified channel. If no small pulse was found at all then both of these new parameters were set to zero.

Prepulses with streamers following so closely that there was no falling edge for the prepulse and it appeared only as a hump on the leading edge of the following streamer (see, for example, the first graph in fig 7.6) could not be distinguished from the streamers themselves, since the pulse-finding algorithm required two falling bins to designate a hit. However, since it had been assumed that any streamer found as the first arriving pulse was an extreme example of this situation in which the streamer had completely swallowed the prepulse, such streamers were included in the timing plots using a combination of PAW cuts.

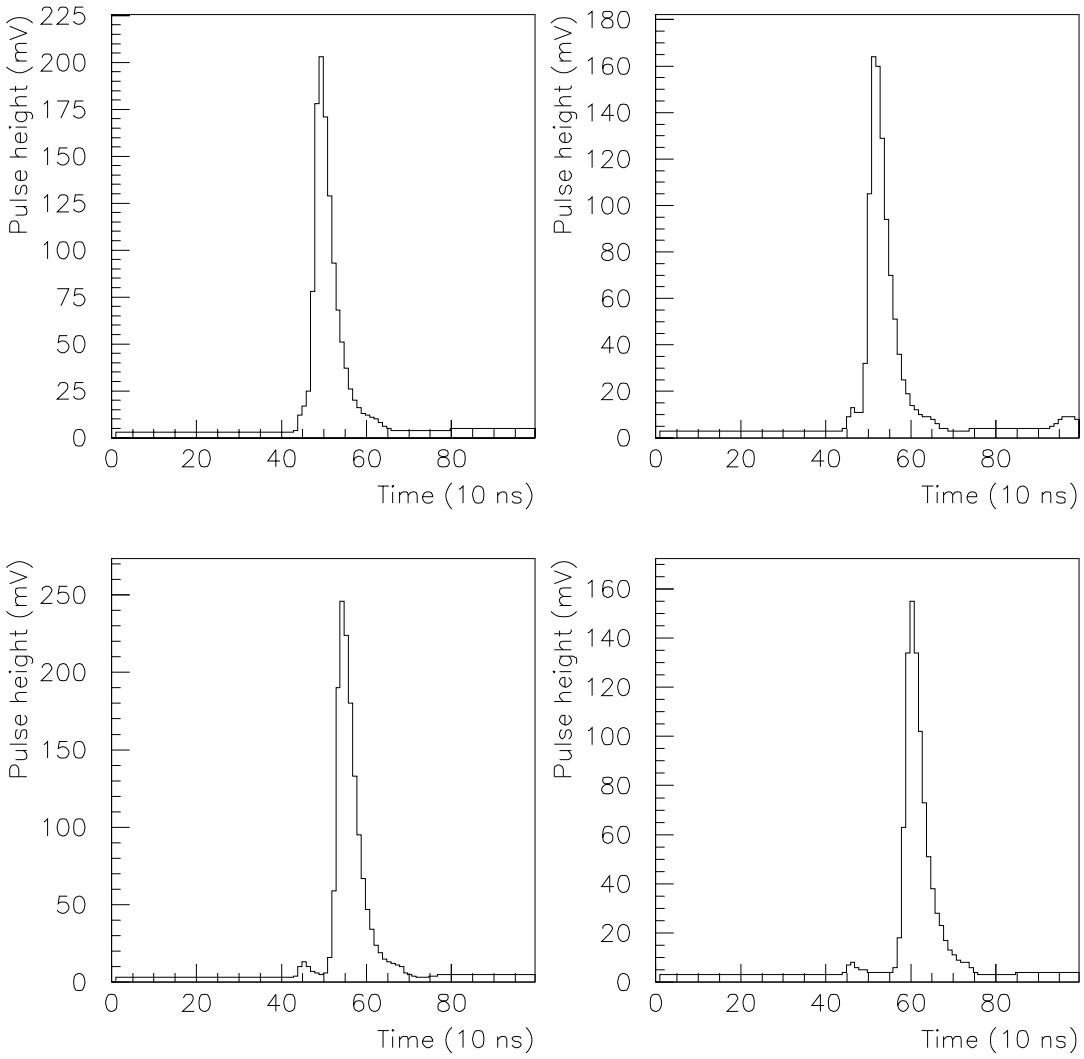

Figure 7.6: FADC digitisings of several events, showing the variation in the separation between the prepulse and the streamer. In the first plot the streamer has arrived so promptly as to overlay the prepulse; in the following plots the streamers arrive later and later with respect to their prepulses.

7.3 Timing plots

The aim of the modification of the program was to make it possible to find out in what way the distributions of the separation in time of streamers from their preceding prepulses varied as the voltage was changed. Past research on RPCs operating in the streamer mode has led to claims of a timing resolution of 1-2 ns, and it remained to be shown that such a resolution was also achievable with the Manchester RPCs in the streamer mode of operation. The prepulse itself arrived with such a good resolution (see figs. 7.1 and 7.2) that the spread in time of the streamers remained the important factor to investigate.

Figures 7.7 and 7.8 show the arrival time of the first large pulse to be found as measured in the unamplified channel for different voltages. This time is found with respect to the time of arrival of the trigger pulse, and as such depends on the differences in the cable lengths between the chambers and the inputs to relevant FADC channel. Taking account of the time necessary for a signal to pass through amplifiers and attenuators, the delays between chamber and FADC input were equalised for all channels, so that the positions of the timing curves on the graphs give a fair indication of the signal time of the RPC with respect to the photomultiplier tube.

The graphs show a systematic decrease in rms, indicating a gradual improvement in resolution with increasing voltage. The best resolution reached is $\sim$ 30 ns, which is far from the 2ns or so expected. The mean also shows a gradual decrease, as the streamers begin to arrive earlier for higher voltages. The skewed Gaussian shape of the distribution becomes sharper as the voltage increases.

The trends in the means and RMS of the distributions are shown figures 7.9 and 7.10.

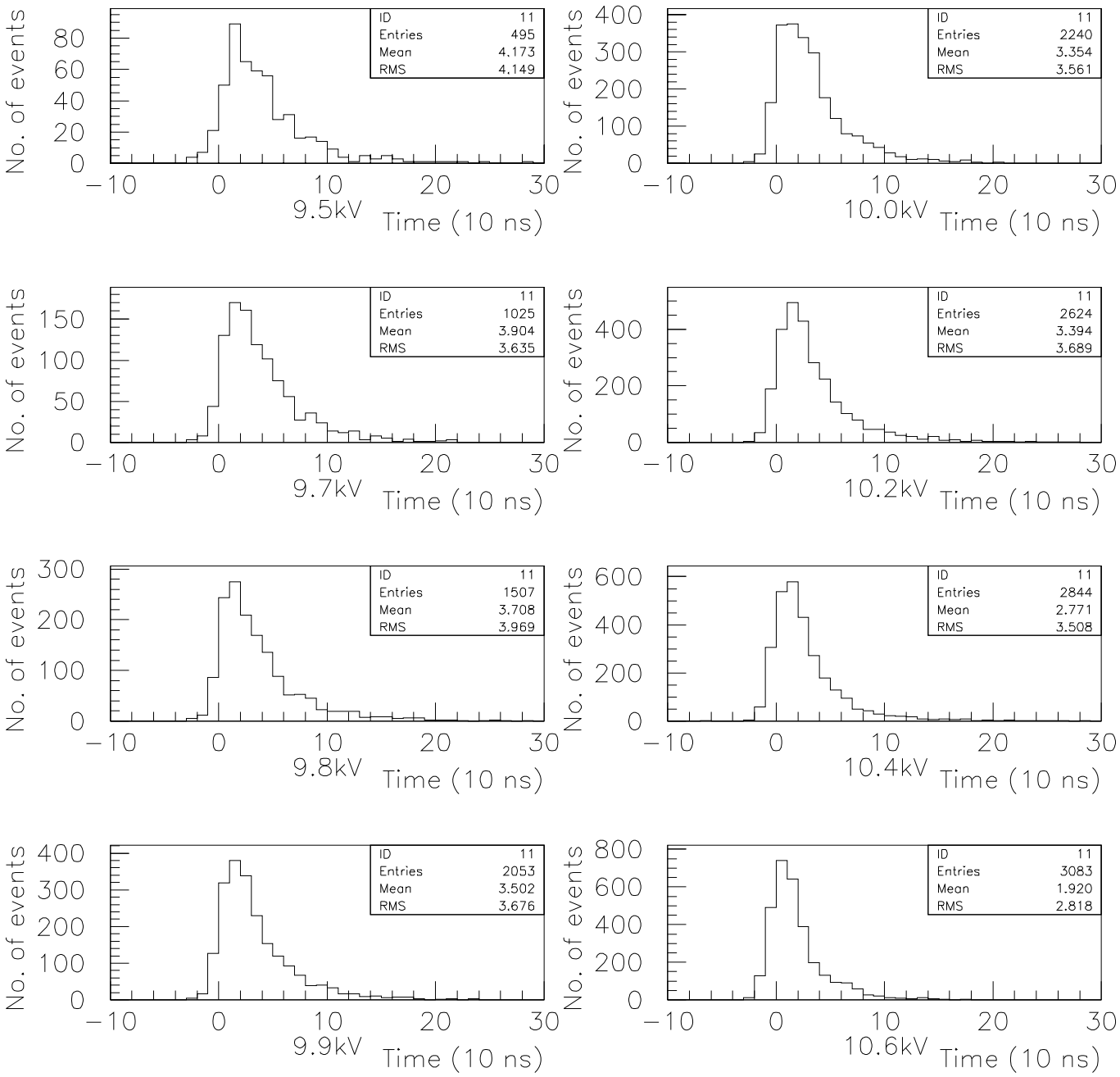

Figure 7.7: Spectra of time of arrival of first large pulse for 3mm chamber.

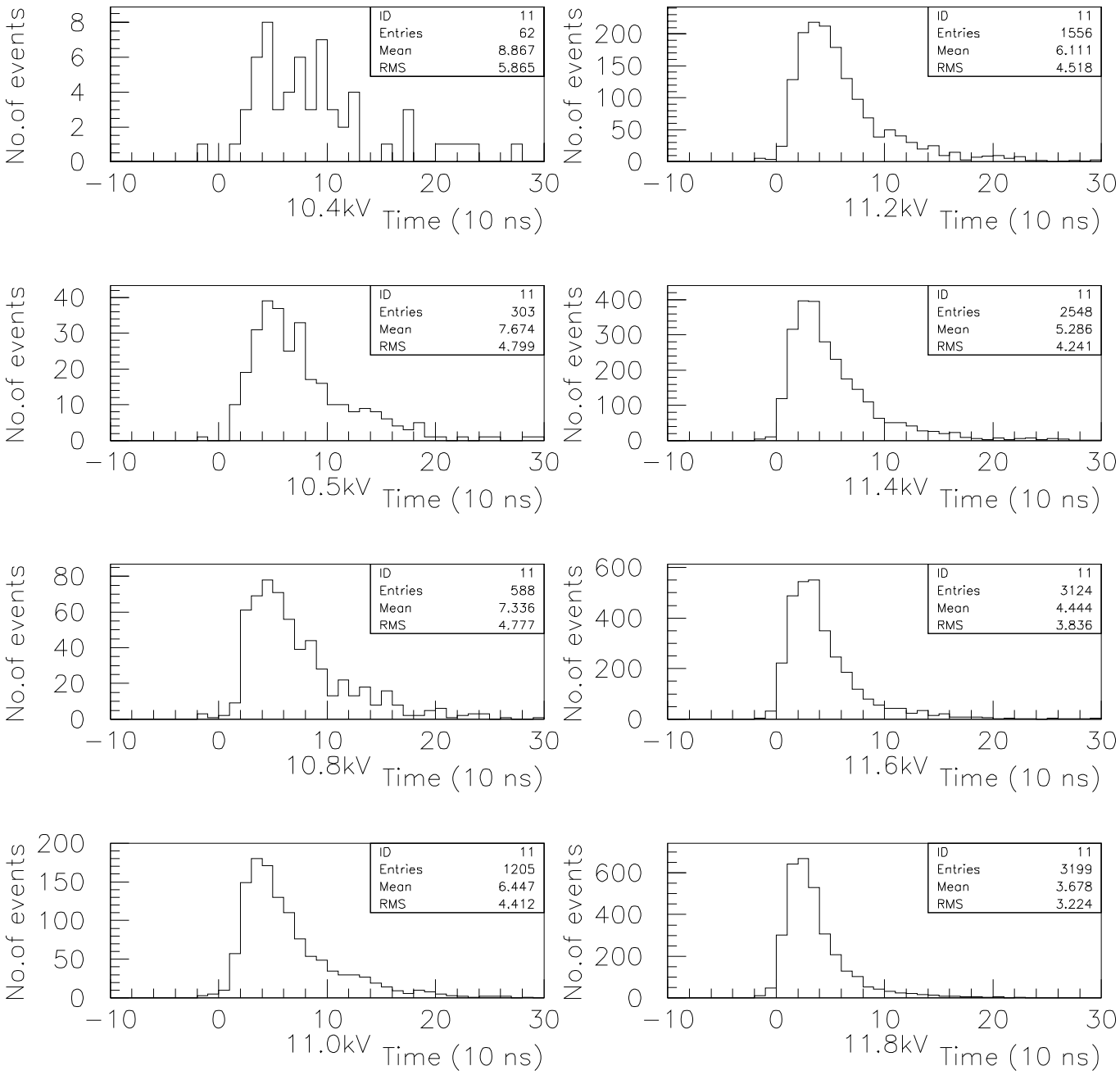

Figure 7.8: Spectra of time of arrival of first large pulse for 4mm chamber.

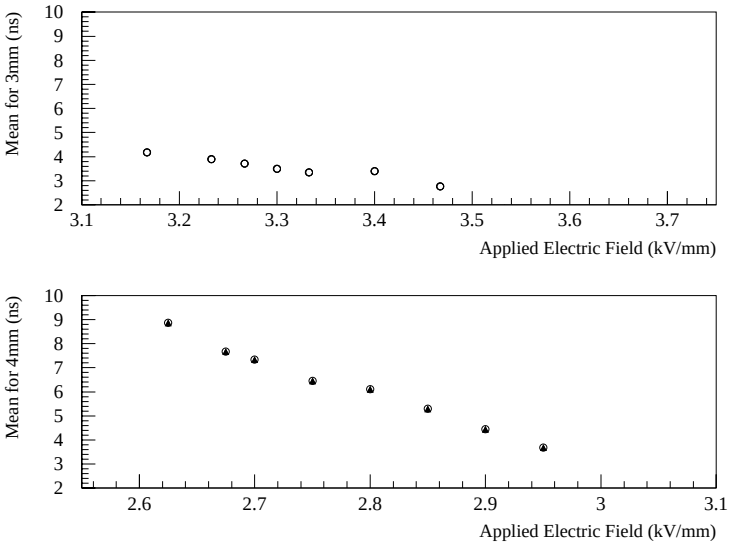

Figure 7.9: The variation in the means of the streamer timing distributions.

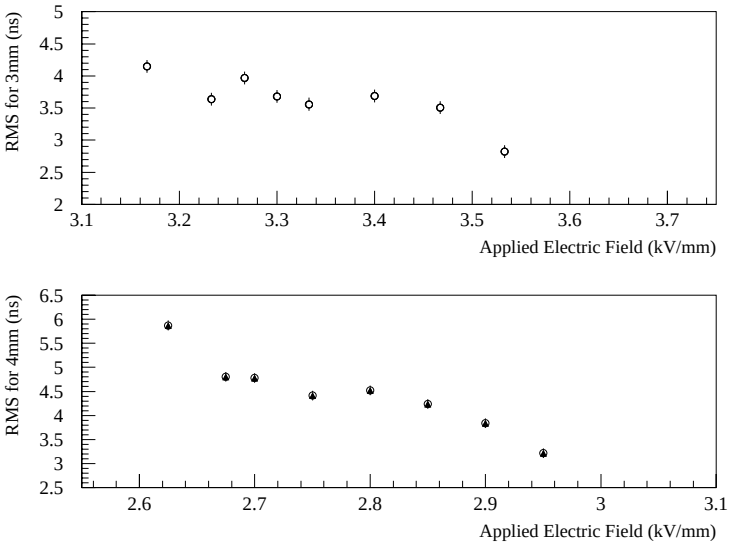

Figure 7.10: The variation in the RMS of the streamer timing distributions.

Chapter 8

Conclusions

8.1 Efficiency

It has been shown that the bakelite RPC is capable of the high efficiencies necessary to satisfy the requirements for a detector at one of the next generation of colliders. Whether it is capable of preserving such an efficiency up to the expected values of the particle flux at the LHC is not certain from the evidence from this project - the data obtained would tend to indicate otherwise, but further work is needed in this area before anything definite can be concluded.

8.2 Timing

The time of arrival of the avalanche pulses with respect to a trigger provides a good demonstration of the reaction-time of the RPCs, and this particular attribute is strong support for their suitability for use in a trigger system. However this reaction-time becomes slower as the size of the gas gap is increased, so that it might not be quite so noticeable for chambers with gaps greater than about 6mm. The distributions of times of arrival of the avalanche pulses show that they arrive promptly and with very little variation. The timing resolution of the avalanche pulses has been shown to reach 3.22 $\pm$ 0.07 ns at 10.2kV for the 3mm RPC, and

3.53 $\pm$ 0.07 ns at 11.6kV for the 4mm RPC. These are somewhat larger than those measured by RD5 [2].

The distributions of the arrival times of the streamer pulses exhibit a great deal of variation - from prompt pulses to streamers arriving 200 ns after the trigger. As the voltage is increased the mean time of arrival of the streamers gradually becomes smaller, indicating that more of the large pulses are arriving earlier.

It was thought that, as the voltage reached higher values, the distributions would begin to assume a Gaussian shape from which the resolution of this type of pulse could be measured. However, the resolution of the streamer pulses as measured in this way is an order of magnitude worse than expected. This is perhaps due to a tendency of the Manchester RPCs to break down before reaching a sufficiently high electric field for such a resolution to be achieved. It is possible that there is a flaw in the analysis software which leads to false identification of pulses such that some streamers which are in fact second-arriving pulses are included in the distribution of first-arriving streamers, and so give rise to a bias towards the tail of late arrivals in the distribution. The trends in the variations in RMS and mean with increasing voltage are comparable to measurements made by N. Morgan et al. [32] using a PVC RPC, and Bencivenni et al. [33] using a glass RPC.

8.3 Rate capability

It can be seen that, in order to be able to cope with the enormous incident fluxes predicted at the next generation of colliders, RPC technology will be forced to abandon one of its previous major selling points - that the signals are large enough not to require preamplification - and instead move towards operating in the avalanche signal mode with the necessity for amplification and associated changes in gas mixtures that that entails. This would however have other benefits such as a possible decrease in the fall off of efficiency with increasing voltage, an effect which has not yet been satisfactorily explained. It is evident that more work needs to be

done before the RPC can fulfill its promise.

8.4 Suggestions for further work

Evidently much further work is needed on RPCs to improve their performance in many areas. With respect to the work at Manchester, the main aim must be to build RPCs that reach a higher and more reliable peak efficiency, and maybe one that is tenable with increasing rate. The effect of dry gases leaching water from the plastic of the resistive plates might prove to be a productive avenue of research, and taking action to prevent this might help to improve the reliability and the efficiency of the chambers. Further research needs to be done to determine a suitable gas mixture for operation in the avalanche mode only.

The trend towards RPCs with wider gas gaps seems to provide a promising avenue for further work, and the investigation of such chambers along the lines of this project might provide more conclusive results than have been obtained here.

The investigation of chambers with strip read-out, rather than a single read-out plate, might also be useful. Study of such chambers would enable work to be done on the spatial resolution of RPCs, and should give shorter pulses with faster rise-times. Also, such chambers should provide the possibilty of gathering information about anode-directed avalanches and cathode-directed avalanches. Comparison of these might lead to some interesting physics, and at the very least should provide evidence to uphold some of the assumptions about electron avalanches and the corresponding drift of positive ions.

Bibliography

[1] R. Santonico and R. Cardarelli, Nucl. Instr. and Meth. 187 (1981) 377.

[2] The RD5 collaboration, ATLAS Internal Note Muon-No-20, 14 May 1993.

[3] L. Antoniazzi et al., Nucl. Instr. and Meth. A315 (1992) 92.

[4] E. Petrolo and S. Veneziano, Nucl. Instr. and Meth. A315 (1992) 95.

[5] D. Cockerill, RPC Workshop, Rome, 1993.

[6] ATLAS Letter of Intent, CERN/LHCC/92-4, 1 October 1992.

[7] Progress Report on ATLAS, Milestones, CERN/LHCC/94–22, 23 May 1994.

[8] R. Cardarelli, A. Di Ciaccio and R. Santonico, Nucl. Instr. and Meth. A333 (1993) 399; R. Cardarelli, Proceedings of the Internatinal Workshop on Resistive Plate Chambers in Particle Physics and Astrophysics, ed. S. Ratti, G. Ciapetti and R. Santonico, Scientifica Acta 8 (1993) 159.

[9] G.L. Bencze et al., "Test of a Resistive Plate Chamber operating with a low gas amplification at high beam", submitted to Nucl. Instr. and Meth.

[10] The RD5 collaboration, Nucl. Instr. and Meth. A340 (1994) 466.

[11] F. Sauli, "Principles of operation of multiwire proportional and drift chambers", CERN 77-09.

[12] Peter Rice-Evans, "Spark, Streamer, Proportional and Drift Chambers", London, 1973.

[13] H. Raether, "Electron Avalanches and Breakdown in Gases", Butterworths, London, 1964.

[14] M. Atac, A.V. Tollestrup and D. Potter, Nucl. Instr. and Meth. 200 (1982) 345.

[15] Phys. Rev. D, volume 45, 1992.

[16] I. Crotty et al., CERN-PPE/94-39.

[17] John Lomas, Manchester HEP Group First Year Report, 1st June 1993.

[18] I. Duerdoth et al., "The Transition from Proportional to Streamer Mode in a Resistive Plate Chamber.", Proceedings of the Third London Conference on Position-Sensitive Detectors, London, September 1993.

[19] Gossen digital flow meter model 5878.

[20] LeCroy discriminator model 621L, coincidence unit model 365AL.

[21] Bertan 10 kV high voltage supply, model 1792P.

[22] Brandenburg 15 kV high voltage supply, model 707R.

[23] LeCroy: linear fan out type 128L, 12 channel PM amplifier model 612A. DNPL-EC attenuator type 241.

[24] NE Fast Octal Discriminator, model 4684.

[25] Hewlett-Packard 54510A digitizing oscilloscope (1 GSa/s).

[26] DL400 100 MHz FADC system, B. Struck, Hamburg.

[27] M. Bertino et al., Nucl. Instr. and Meth. A283 (1989) 654.

[28] I. Crotty et al., Nucl. Instr. and Meth. A239 (1993) 133.

[29] S. D. Kolya, "Development DAQ system", Manchester University internal report, 1990.

[30] S. D. Kolya, "Processing Code in DC FEPs", Manchester University internal report, 1990.

[31] J. M. Foster, private communication.

[32] N. Morgan et al., Nucl. Instr. and Meth. A340 (1994) 341.

[33] G. Bencivenni et al., Nucl. Instr. and Meth. A332 (1993) 368.

Acknowledgements

I would like to thank everyone who has helped me this year in one way or another; especially to Fred, Ian, Ray, Julian and Joe, for discussions, explanations, and the ceremonial laying-on of hands to make things work. Also thanks to Crispin, Ian and Pepe for letting me play with their detectors at CERN.

And of course, many many thanks to my parents for their support - financial and otherwise - throughout this year.